

1 Supporting information for: Wilson *et al.* 2022. The role of spatial  
2 structure in at-risk metapopulation recoveries. In: *Ecological*  
3 *Applications*.

4 **Appendix S1:** Overview of metapopulation model description & detailed results

5 Kyle L. Wilson<sup>1,2\*</sup>; Alexandra C. Sawyer<sup>1</sup>, Anna Potapova<sup>1</sup>, Colin J. Bailey<sup>1</sup>, Daniella LoScerbo<sup>3,4</sup>,  
Elissa K. Sweeney-Bergen<sup>1,5</sup>, Emma E. Hodgson<sup>1,4</sup>, Kara J. Pitman<sup>1</sup>, Karl M. Seitz<sup>1</sup>,  
Lauren Law<sup>1,6</sup>, Luke Warkentin<sup>1,7</sup>, Samantha M. Wilson<sup>1</sup>, William I. Atlas<sup>1,8</sup>,  
Douglas C. Braun<sup>3,5</sup>, Matthew R. Sloat<sup>8</sup>, M. Tim Tinker<sup>9</sup>,  
and Jonathan W. Moore<sup>1,3</sup>

<sup>1</sup>Earth to Ocean Research Group, Simon Fraser University

<sup>2</sup>Central Coast Indigenous Resource Alliance, Campbell River, BC

<sup>3</sup>Resource and Environmental Management, Simon Fraser University

<sup>4</sup>Fisheries & Oceans Canada, Cultus Lake Laboratory, Cultus Lake, BC

5 Ministry of Forests, Lands, Natural Resource Operations, and Rural Development, Smithers, BC

<sup>6</sup>Fisheries & Oceans Canada, Salmonid Enhancement Program, Nanaimo, BC

<sup>7</sup>Fisheries & Oceans Canada, North Coast Stock Assessment, Smithers, BC

<sup>8</sup>Wild Salmon Center, Portland, OR

<sup>9</sup>Ecology and Evolutionary Biology, University of California Santa Cruz

6 16 December 2022

7 **Contents**

S1.1 Metapopulation model . . . . .	2
S1.1.1 Local & metapopulation dynamics . . . . .	2
S1.1.2 Creating the spatial networks . . . . .	3
S1.1.3 Dispersal . . . . .	4
S1.1.4 Disturbance regimes . . . . .	5
S1.1.5 Recruitment stochasticity . . . . .	6
S1.2 Post-disturbance outcomes . . . . .	7
S1.2.1 Monitoring & management at aggregate-scale . . . . .	7
S1.2.2 Recovery metrics . . . . .	8
S1.3 Scenarios . . . . .	8
S1.3.1 Walkthrough of example results . . . . .	10
S1.4 Sensitivity test of mean recovery metrics . . . . .	16
S1.5 General patterns . . . . .	17
S1.5.1 Effects of disturbance regime . . . . .	17
S1.5.2 Role of network structure & dispersal . . . . .	18
S1.5.3 Clustering analyses . . . . .	23
S1.5.4 Emergent recovery outcomes . . . . .	24
S1.6 References . . . . .	29

\*Corresponding author - email: klwilson.ccira@gmail.com

26 **S1.1 Metapopulation model**

27 **S1.1.1 Local & metapopulation dynamics**

28 Our metapopulation was defined by a set of  $P$  local populations for a species with a one year generation time with  
 29 time-dynamics that follows birth (i.e., recruitment  $R$ ), immigration, death, and emigration processes typical to  
 30 metapopulation theory and tested the role of multiple local and regional processes (Anderson *et al.* 2015; Fullerton  
 31 et al. 2016; Zelnik *et al.* 2019; Bowlby & Gibson 2020; Okamoto *et al.* 2020):

$$N_{i,t} = (1 - d_{i,t})(R_{i,t} + \sum_{\substack{j=1 \\ j \neq i}}^P \omega p_{i,j} R_{j,t} - \omega R_{i,t}) \quad (\text{S.1})$$

32 where  $N_{i,t}$  was the number of adults in patch  $i$  at time  $t$ ,  $R_{i,t}$  was the number of recruits at time  $t$ ,  $\sum_{\substack{j=1 \\ j \neq i}}^P \omega p_{i,j} R_{j,t}$  was  
 33 the number of recruits immigrating into patch  $i$  from any other patch,  $\omega$  was the proportion of local recruits to  
 34 disperse,  $p_{i,j}$  was a distance-dependent dispersal function, and  $d_{i,t}$  was the proportion of post-dispersal recruits lost  
 35 from the disturbance regime.

36 Figure S1 shows how local patch recruitment at time  $t$  depended on adult densities at  $t-1$  and followed a  
 37 reparameterized Beverton-Holt function based on compensation ratio (see Box 3.1 in Walters & Martell 2004) and  
 38 ignoring age-structure to model adult-to-adult dynamics, i.e., setting  $\phi_{E_0} = 1$ ,  $\phi_{B_0} = 1$  and  $R_0 = N_0$  (see Table 3 in  
 39 Forrest *et al.* 2010):

$$R_{i,t} = \frac{\alpha_i N_{i,t-1}}{1 + \frac{\alpha_i - 1}{\beta_i} N_{i,t-1}} \epsilon_{i,t} \quad (\text{S.2})$$

40 where  $\alpha_i$  was the recruitment compensation ratio,  $\beta_i$  was local patch carrying capacity, and  $\epsilon_{i,t}$  was lognormally  
 41 distributed deviates to introduce stochastic recruitment dynamics.

42 Resource monitoring often occurs at the scale of the whole metapopulation by sampling aggregate abundances from  
 43 multiple local populations to (Anderson *et al.* 2015; Moore *et al.* 2021), hence we define metapopulation adults as:

$$A_t = \sum_{i=1}^P N_{i,t} \quad (\text{S.3})$$

44 with metapopulation recruits:

$$K_t = \sum_{i=1}^P R_{i,t} \quad (\text{S.4})$$

45 Monitoring at the scale of the whole metapopulation can produce productivity relationships that aggregates the  
 46 population dynamics and productivity among all local populations. For example, take a two patch metapopulation  
 47 model (Figure S1) that each vary in demographic shape parameters  $\alpha_1 = 2$ ;  $\alpha_2 = 4$  and  $\beta_1 = 100$ ;  $\beta_2 = 200$ . Here,  
 48 recruitment compensation from local patches  $\alpha_i$  gets averaged across the metapopulation leading to an average  
 49 compensation ratio  $\bar{\alpha}$  of 3. Likewise, the total carrying capacity of the metapopulation  $\bar{\beta}$  becomes the summation  
 50 of local patch carrying capacities  $\sum \beta_i$ , which was 300. This scale of monitoring generates the following local patch  
 51 and metapopulation dynamics:

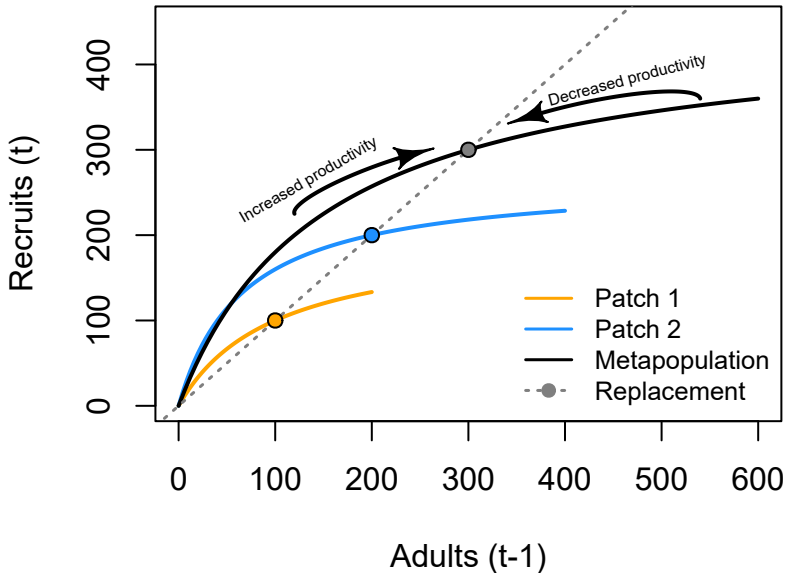


Figure S1: Density dependence in metapopulation and local patch recruitment dynamics. Dashed line indicates the line of replacement, with equilibrium indicated by points. When populations fall below equilibrium points, per-capita productivity improves driving populations back towards equilibrium. When populations exceed their capacity, per-capita productivity decreases driving populations back towards equilibrium. At each point of the x-axis, the distance between the solid and dashed lines indicates the amount of recruitment above replacement, i.e., the surplus recruitment produced via compensatory density dependence.

### 52 S1.1.2 Creating the spatial networks

53 The next aspect to developing our metapopulation model was connecting the set of patches to one another (Yeakel  
 54 et al. 2014). We needed to specify the number of patches, their arrangements (i.e., connections), and how far apart  
 55 they are from one another. We followed some classic metapopulation and source-sink arrangements to create four  
 56 networks that generalize across a few real-world topologies: a linear habitat network (e.g., coastline), a dendritic or  
 57 branching network (e.g., coastal rivers), a star network (e.g., mountain & valley, or lake with inlet tributaries), and  
 58 a grid network (e.g., grasslands).

59 To make networks comparable, each spatial network type needs the same leading parameters (e.g., number of  
 60 patches  $P$  and mean distance between neighboring patches  $\bar{d}$ ). In this case, we set  $P$  to 16 and  $\bar{d}$  to 1 unit  
 61 (distance units are arbitrary). We used the `igraph` package (Csardi & Nepusz 2006) to arrange our spatial  
 62 networks as the following:

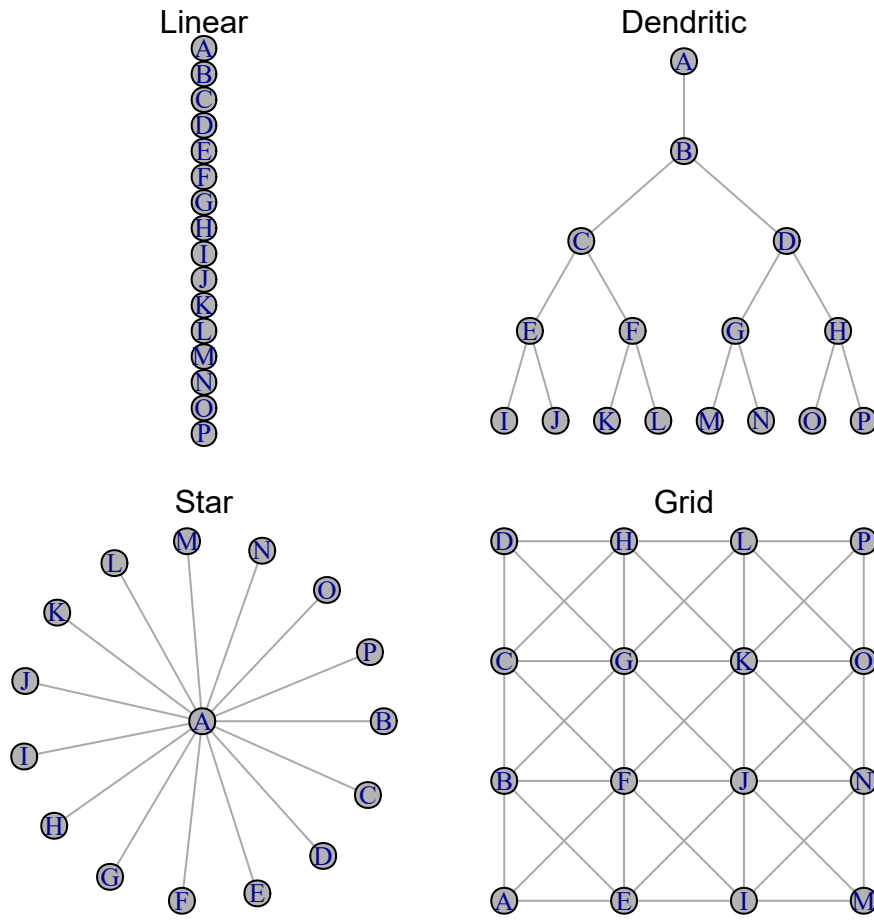


Figure S2: Four spatial network topologies.

<sup>63</sup> Note that distances between neighbor patches in the above networks are equal. Table S1 shows an example  
<sup>64</sup> dispersal matrix for a grid network.

### <sup>65</sup> S1.1.3 Dispersal

<sup>66</sup> Dispersal from patch  $i$  into patch  $j$  depends on constant dispersal rate  $\omega$  (defined as the proportion of total local  
<sup>67</sup> recruits that will disperse) and an exponential distance-decay function between  $i$  and  $j$  with distance cost to  
<sup>68</sup> dispersal  $m$  (Anderson et al. 2015; Fullerton et al. 2016):

$$E_{i,j,t} = \omega R_{i,t} p_{i,j} \quad (\text{S.5})$$

<sup>69</sup> where  $E_{i,j}$  was the total dispersing animals from patch  $i$  into patch  $j$  resulting from dispersal rate  $\omega$ , total number  
<sup>70</sup> of local recruits  $R_{i,t}$ , and probability of dispersal between patches  $p_{i,j}$ :

$$p_{i,j} = \frac{e^{-md_{i,j}}}{\sum_{\substack{j=1 \\ j \neq i}}^P e^{-md_{i,j}}} \quad (\text{S.6})$$

<sup>71</sup> where  $d_{i,j}$  was the pairwise distance between patches,  $m$  was the distance cost to dispersal. The summation term in  
<sup>72</sup> the denominator normalizes the probability of moving to any patch to between 0 and 1 with the constraint that

Table S1: Example distance matrix between 16 patches within a grid network to affect distance-dependent dispersal rates.

	A	B	E	F	C	G	D	H	I	J	K	L	M	N	O	P
A	0	1	1	1	2	2	3	3	2	2	2	3	3	3	3	3
B	1	0	1	1	1	1	2	2	2	2	2	2	3	3	3	3
E	1	1	0	1	2	2	3	3	1	1	2	3	2	2	2	3
F	1	1	1	0	1	1	2	2	1	1	1	2	2	2	2	2
C	2	1	2	1	0	1	1	1	2	2	2	2	3	3	3	3
G	2	1	2	1	1	0	1	1	2	1	1	1	2	2	2	2
D	3	2	3	2	1	1	0	1	3	2	2	2	3	3	3	3
H	3	2	3	2	1	1	1	0	3	2	1	1	3	2	2	2
I	2	2	1	1	2	2	3	3	0	1	2	3	1	1	2	3
J	2	2	1	1	2	1	2	2	1	0	1	2	1	1	1	2
K	2	2	2	1	2	1	2	1	2	1	0	1	2	1	1	1
L	3	2	3	2	2	1	2	1	3	2	1	0	3	2	1	1
M	3	3	2	2	3	2	3	3	1	1	2	3	0	1	2	3
N	3	3	2	2	3	2	3	2	1	1	1	2	1	0	1	2
O	3	3	2	2	3	2	3	2	2	1	1	1	2	1	0	1
P	3	3	3	2	3	2	3	2	3	2	1	1	3	2	1	0

73 dispersers cannot move back into their home patch (i.e.,  $j \neq i$ . With  $\bar{d} = 1$ ,  $m = 0.5$ ,  $\omega = 0.1$ ,  $R_{i,t} = 100$  in a linear  
74 network):

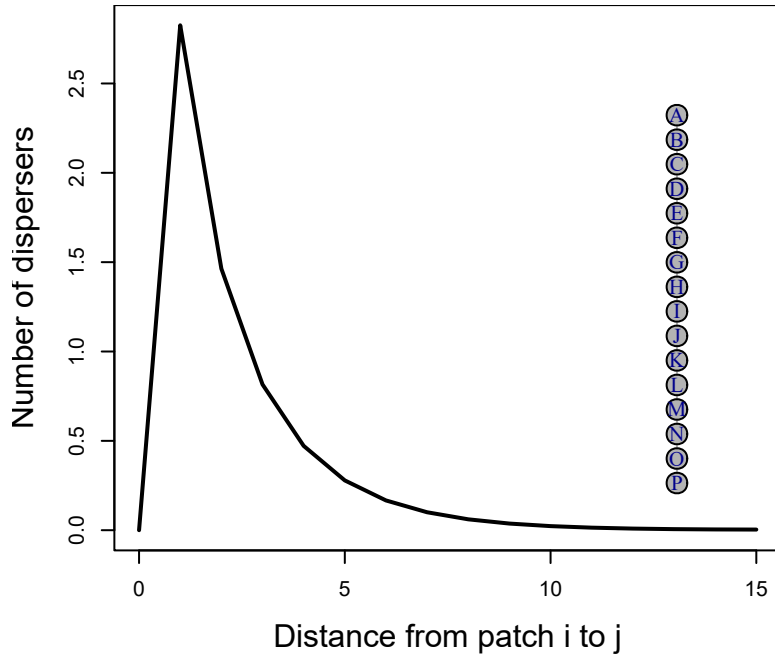


Figure S3: Example dispersal patterns across linear network.

#### 75 S1.1.4 Disturbance regimes

76 In all scenarios, disturbance was applied after 50 years of equilibrating the metapopulation at pristine conditions.  
77 We then applied a pulsed disturbance regime at year 50 (the regime varied from *uniform*, *localized*, *even*, and  
78 *localized, uneven* - see *Scenarios* below). Disturbance immediately removed a fixed proportion of the  
79 metapopulation adults at that time (i.e., 0.9 of  $A_{t=50}$ ). Once applied, the metapopulation was no longer disturbed

and spatio-temporal recovery dynamics emerged from these conditions given the ecological scenarios of network complexity, dispersal rate, spatio-temporal correlations, local patch demographies, and magnitude of stochastic variance.

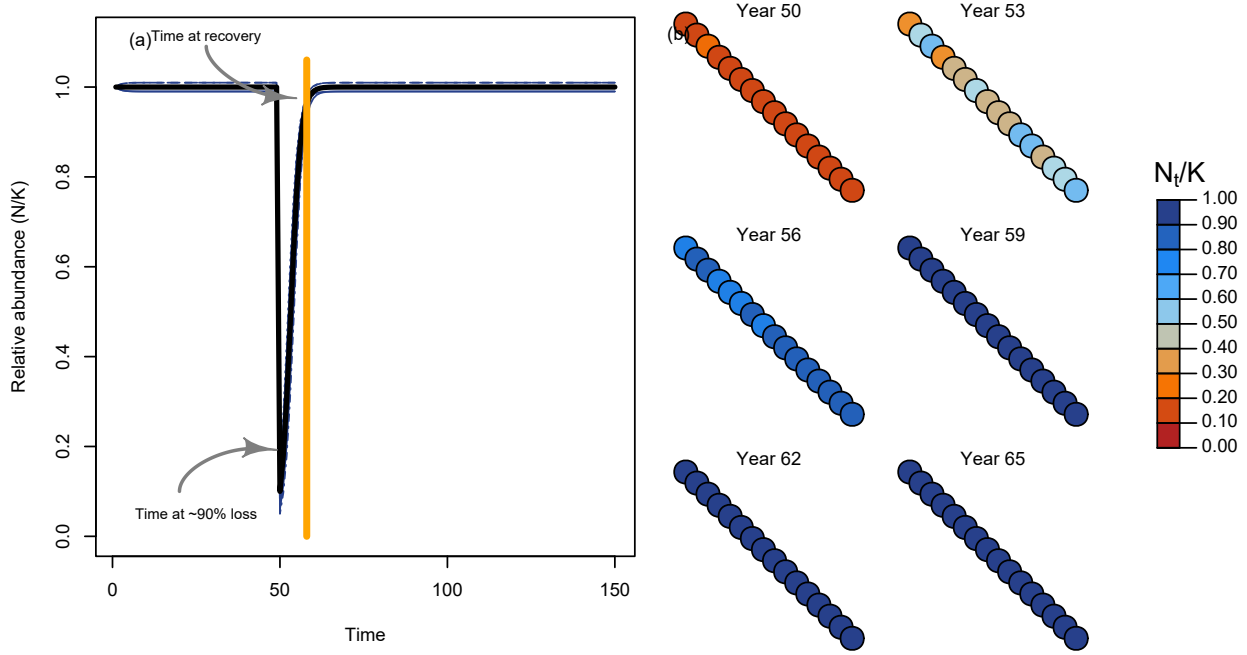


Figure S4: Recovery regime of metapopulation with linear topology through time (a) and space (b).

### S1.1.5 Recruitment stochasticity

Our model allowed for stochastic recruitment that followed a lognormal distribution with average variation in recruitment of  $\sigma_R$ . In cases with stochastic recruitment, the deterministic recruitment in eq. S.4 becomes:

$$R_{i,t} = \frac{\alpha_i N_{i,t-1}}{1 + \frac{\alpha_i - 1}{\beta_i} N_{i,t-1}} e^{(\epsilon_{i,t} - \frac{\sigma_R^2}{2})} \quad (\text{S.7})$$

where lognormal deviates for each patch  $i$  at time  $t$  were drawn from a multivariate normal distribution ( $MVN$ ) with bias correction  $\frac{\sigma_R^2}{2}$ . If  $\sigma_R$  was low, then metapopulation dynamics approach the deterministic case. In some scenarios, we evaluated the role of spatially and/or temporally correlated deviates among local patches to model potential common drivers affecting metapopulation dynamics (e.g., Moran effects). Expected recruitment deviates followed a first-order autoregression model such that:

$$\epsilon_{i,t} = \rho_T \epsilon_{i,t-1} + MVN(\mu = 0, \Sigma = \sigma_R^2(1 - \rho_T^2)e^{(-\rho_S D_{i,j})}) \quad (\text{S.8})$$

where  $\rho_T$  was temporal correlation (bounded 0 – 1) and  $\rho_S$  was rate of distance-decay in spatial correlation (bounded 0 –  $\infty$  with higher values leading to independent patches). If  $\rho_T$  was 0 and  $\rho_S$  was high, then annual recruitment deviates were independent. We modelled the initial conditions for autoregressive recruitment deviates  $\epsilon_{i,1}$  by drawing from a stationary normal distribution with mean  $\mu = 0$  and variance  $\sigma_R^2$  such that:

$$\epsilon_{i,1} \sim N(\mu = 0, \sigma = \sigma_R) \quad (\text{S.9})$$

We illustrate the effects of four kinds of recruitment deviates below using the same random number generator seed:

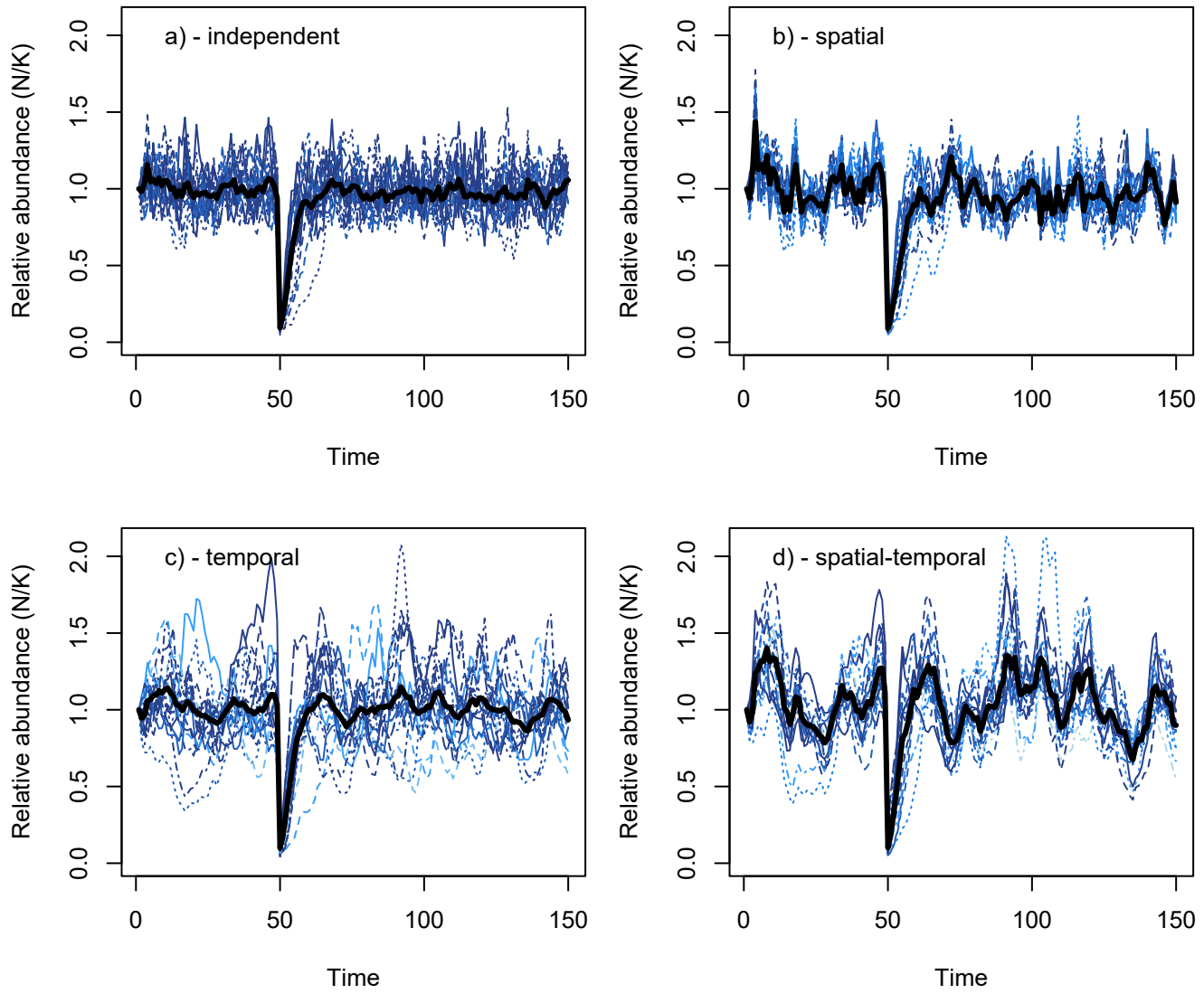


Figure S5: Metapopulation dynamics with independent (a), spatially correlated (b), temporally correlated (c), and spatio-temporally correlated (d) recruitment deviates. Black line indicates metapopulation, and dashed lines indicate local patches with red and blue relating to abundances after 100 years post-disturbance were less than or greater than 1.0 pre-disturbance, respectively.

## 92 S1.2 Post-disturbance outcomes

### 93 S1.2.1 Monitoring & management at aggregate-scale

94 While true metapopulation dynamics emerge from local patch dynamics and dispersal in eq. S.1, natural resource  
 95 managers often monitor and manage at the scale of the metapopulation. Hence, management at this scale  
 96 inherently defines the stock-recruitment dynamics of the aggregate complex of patches (i.e., metapopulation) as:

$$\mathbb{E}(N_t) = \frac{\bar{\alpha}A_{t-1}}{1 + \frac{\bar{\alpha}-1}{\bar{\beta}}A_{t-1}} \quad (\text{S.10})$$

97 where  $\bar{\alpha}$  was the compensation ratio averaged across the metapopulation and  $\bar{\beta}$  was the carrying capacity summed  
 98 across the entire metapopulation.

### 99 S1.2.2 Recovery metrics

100 We measured the following post-disturbance outcomes to track the temporal and spatial recovery regime of the  
101 metapopulation.

- 102 1. Recovery rate after disturbance: Recovery rate represents the inverse proportion of the post-disturbance  
103 phase that the metapopulation took to recover. Recovery rate was calculated as  $1 - T_{recovery}/T_{sim}$  where the  
104 recovery time,  $T_{recovery}$ , was the number of years/generations (1 year = 1 generation in our models) it took  
105 for the metapopulation to reach five consecutive years pre-disturbance abundance. Recovery rate captures  
106 how quickly the aggregate metapopulation recovers from disturbance but doesn't take into account whether  
107 any given local patches recover to their pre-disturbance capacity nor did it allow for any uncertainty around  
108 recovery criteria.
- 109 2. Patch occupancy: The number of patches with >0.1 local carrying capacity after disturbance in the  
110 short-term (5 years), medium-term (10 years), and long-term (25 years). This value characterizes the  
111 expected risk of spatial contractions or local patch collapses, and reflects how interactions between spatial  
112 structure, disturbance, and dispersal shape source-sink dynamics and the ability to provide (or not) rescue  
113 effects and recover local patches.
- 114 3. Relative production: The ratio between the empirical metapopulation adult abundances to the expected adult  
115 recruitment if the metapopulation were a single, contiguous population of equivalent size and productivity  
116 (i.e., carrying capacities and productivity were equal to the sum  $\beta$  and mean  $\alpha$  among patches, respectively).  
117 We term  $\Delta_N$  by calculating the stock-recruitment model to aggregate metapopulation adults (eq. S.10) such  
118 that:

$$\Delta_{N_t} = \frac{A_t}{\mathbb{E}(N_t)} \quad (\text{S.11})$$

119 A value of 1.0 would indicate that the disturbed metapopulation production was equal to a single, contiguous  
120 population such that source-sink dynamics were not consuming surplus recruits. In other words, this metric  
121 can describe whether the metapopulation acts more than ( $\Delta_{N_t} > 1.0$ ), less than ( $\Delta_{N_t} < 1.0$ ), or equal to the  
122 sum of its parts ( $\Delta_{N_t} = 1.0$ ).

- 123 4. Risk of non-recovery after disturbance: Non-recovery rate was defined as the % of simulations where  
124 metapopulation abundance failed to recover to 1.0 of the average pre-disturbance abundance for 5  
125 consecutive years post-disturbance. This "non-recovery rate" reflects the risk of a long-term state shift in  
126 metapopulation dynamics after disturbance in the face of stochasticity.

### 127 S1.3 Scenarios

128 We tested all combinations of the following eight processes (below) and ran 100 stochastic iterations per scenario  
129 (see section on *Sensitivity test of mean recovery metrics* below) to estimate the mean outcome for each of the above  
130 recovery metrics:

- 131 1. Homogenous and spatially variable recruitment compensation ratio across patches, i.e. intrinsic rate of  
132 population growth ( $\alpha_i$ ).
  - 133 a. when **variable**,  $\alpha_i \sim TN(\mu = \bar{\alpha}, \sigma_\alpha = 0.3\bar{\alpha})$  with a truncation applied such that  $5 \leq \alpha_i \geq 1$  to ensure  
134 that patches could, at minimum, could replace themselves but with an upper limit of a 5-fold  
135 improvement to per-capita productivity. By comparison, Myers et al. (1999) found that compensation  
136 ratio (their  $\hat{\alpha}$ ) ranged 1-7 for most species evaluated. Since our focus was on at-risk species, we opted to  
137 truncate  $\alpha_i$  towards the lower end of this range, with a mean of 2.0.
- 138 2. Homogenous and spatially variable local carrying capacity across patches, i.e. asymptote of expected recruits  
139 at high adult densities ( $\beta_i$ )
  - 140 a. when **variable**,  $\beta_i \sim multinomial(p_i, N)$  where  $p_i = \frac{e^{\theta_i}}{\sum e^{\theta_i}}$ ,  $\theta_i \sim uniform(0, 1)$ , and  $N = \bar{\beta}$ , with the  
141 added constraint that  $\beta_i < 0.1\bar{\beta}$  to ensure that no one patch exceed 10% of total metapopulation  
142 abundance (a necessary constraint when modelling *local, even* and *local, uneven* disturbances below).  
143 Note that, when local variation in demography rates occurred, the truncated normal in *Appendix S1: Section 1.3.1.a* and truncated multinomial in *Appendix S1: Section 1.3.2.a* above led compensation ratio  
144 and carrying capacity, respectively, to vary by the same magnitude ~28% coefficient of variation  
145 (Appendix S1: Figure S6).

- 147 3. Variation in the spatial distribution of disturbances where a proportion of individuals were removed from the  
148 metapopulation (e.g., 0.90) occurs.
- 149   a. *uniform* - individuals randomly removed across all patches, with all individuals having equal  
150 vulnerability to being removed.
- 151   b. *local, even* - randomly chosen individuals removed from random subset of patches (as long as the target  
152 individuals lost in the metapopulation can be achieved in that subset of patches)
- 153     i. Specifically, a numerical algorithm was used to search and find a set of disturbance conditions  
154       whereby removing a random proportion of individuals from a random subset of local patches  
155       achieved both:  
156         • a total loss that summed to a ~90% loss in abundance to the whole metapopulation, and  
157         • left at least one local patch *undisturbed* to start metapopulation recoveries.
- 158   c. *local, uneven* - total extirpation of randomly selected subset of patches (as long as the target individuals  
159       lost in the metapopulation can be achieved in that subset of patches).
- 160     i. Specifically, a numerical algorithm was used to search and find a set of disturbance conditions  
161       whereby extirpations to a random subset of local patches achieved both:  
162         • a total loss that summed to a ~90% loss in abundance to the whole metapopulation, and  
163         • left at least one local patch *undisturbed* to start metapopulation recoveries.
- 164 4. Density-independent dispersal rates  $\omega$  from 0 to 5% of individuals within a patch will disperse.
- 165 5. Topology of the spatial networks with linear, dendritic, star, and grid networks. Each network with  $P = 16$   
166 and distance between patches  $\bar{d} = 1$ .
- 167 6. Stochastic recruitment deviates with low, medium, and high standard deviation in lognormal error. Used to  
168 generate stochastic population dynamics via random deviates from the expected recruitment relationship in  
169 eq. S.2.
- 170 7. Temporal correlation in recruitment deviates from low, medium, and high correlation (i.e., good year at time  
171  $t$  begets good year at time  $t+1$ ).
- 172 8. Spatial correlation in recruitment deviates among patches from low, medium, to high correlation (i.e.,  
173 neighboring patches go up or down together).

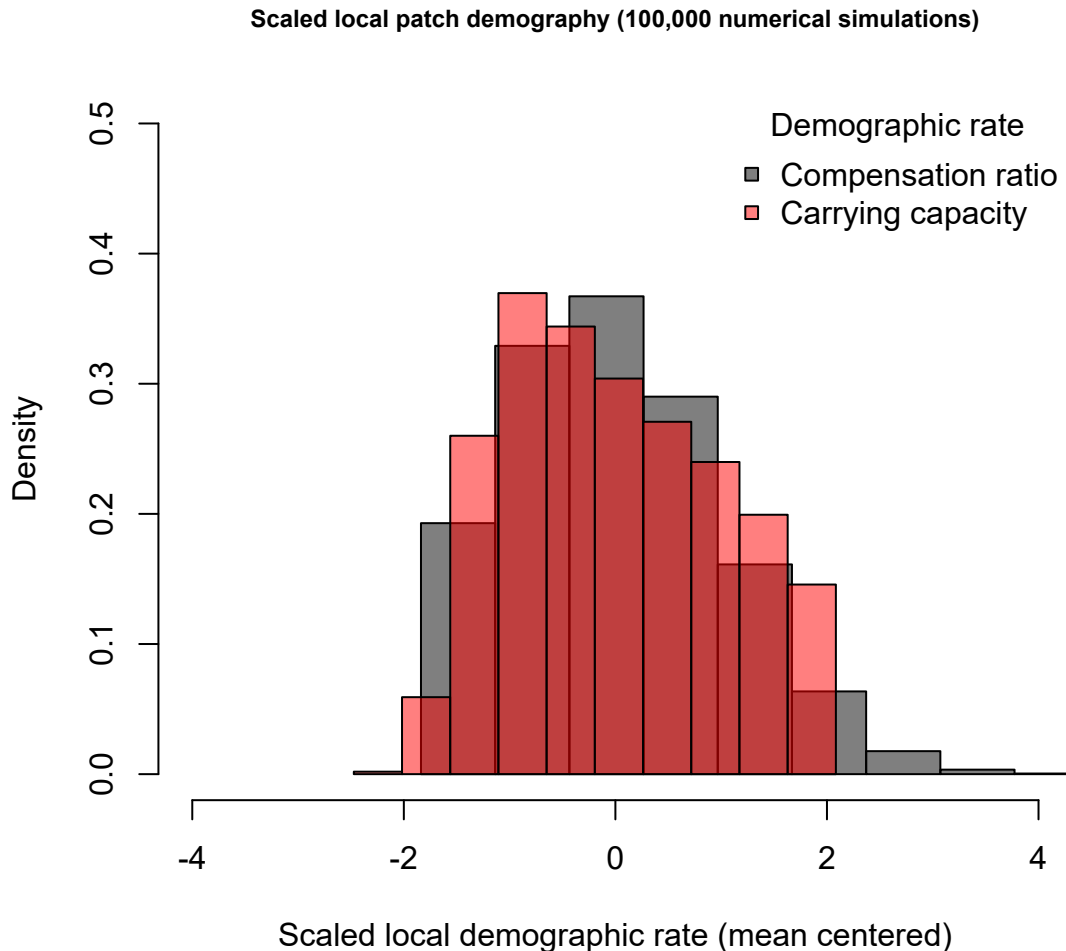


Figure S6: Histogram showing variation among demographic rates after simulating 100,000 local patches when using the truncated normal in Appendix S1: Section 1.3.1.a and truncated multinomial in Appendix S1: Section 1.3.2.a when modelling variation in local compensation ratio (grey) and carrying capacity (red).

<sup>174</sup> **S1.3.1 Walkthrough of example results**

<sup>175</sup> We demonstrate our metapopulation model with an example outcome for a linear network composed of 16 patches,  
<sup>176</sup> a dispersal rate of 0.01 and a high enough dispersal cost such that individuals are only willing to move to their  
<sup>177</sup> closest neighboring patches. This limits the strength of potential rescue effects. For this example, patches varied in  
<sup>178</sup> their productivity and carrying capacity but will have deterministic population dynamics.

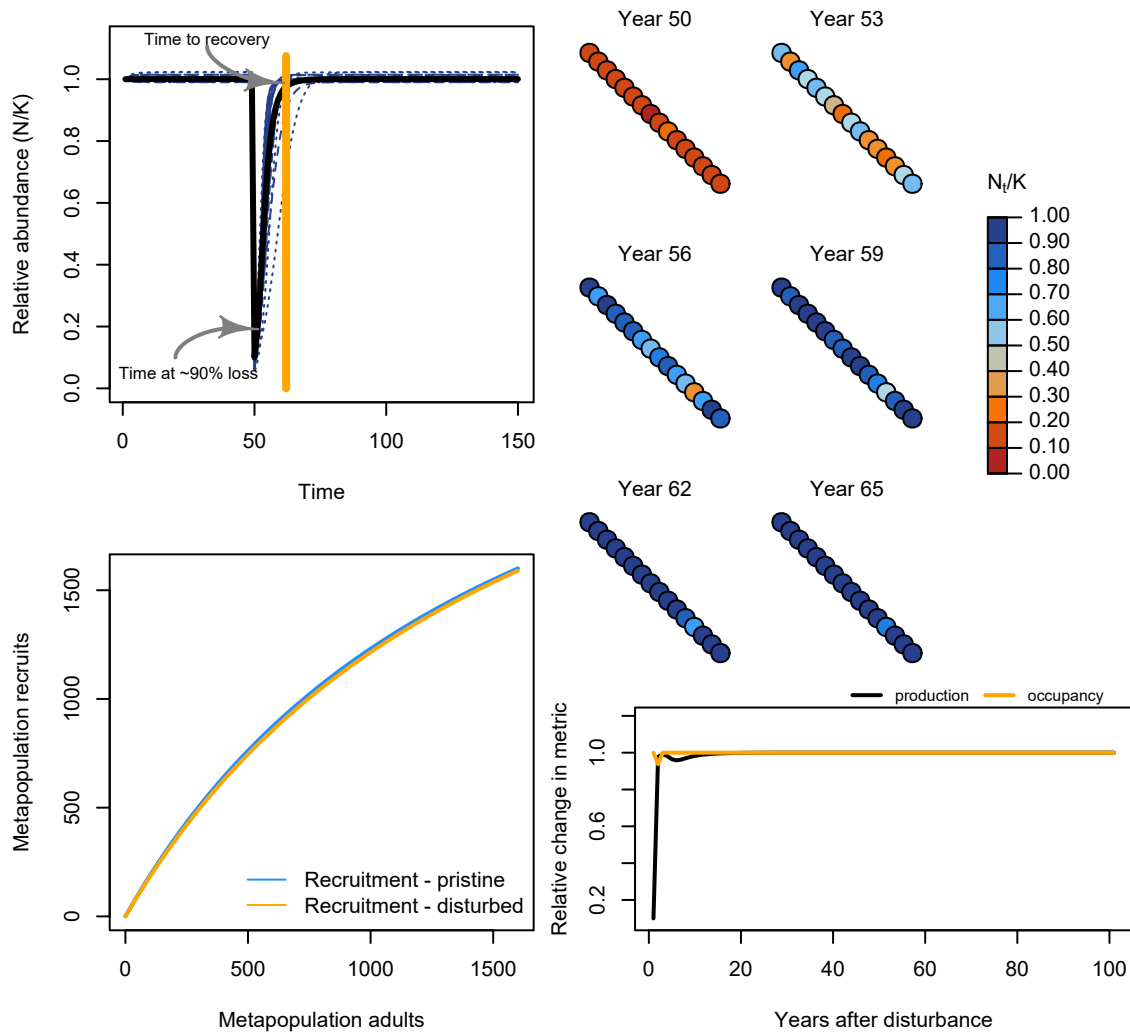


Figure S7: Example iteration of spatial recovery regime of metapopulation with linear topology through time (top left) and space (top right). Recruitment dynamics before and 10 years after disturbance (bottom left). Relative bias in aggregate-scale estimates of carrying capacity, compensation ratio, and recruitment production in recovery phase (bottom right).

<sup>179</sup> We can then contrast this with a different network shape, like a dendritic network.

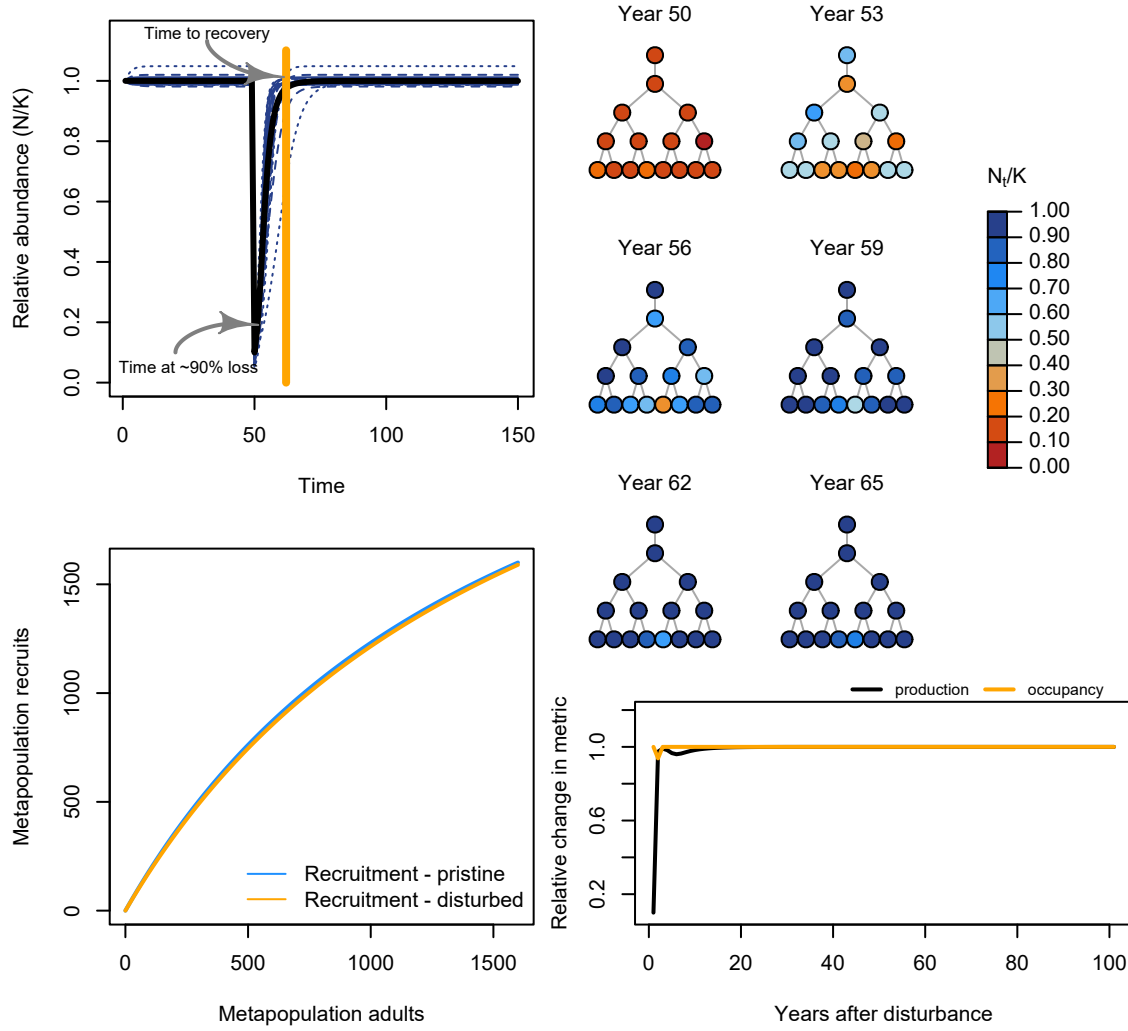


Figure S8: Example iteration of spatial recovery regime of metapopulation with dendritic topology.

<sup>180</sup> Now, let's add some stochasticity to recruitment and see how this affects the recovery regime.

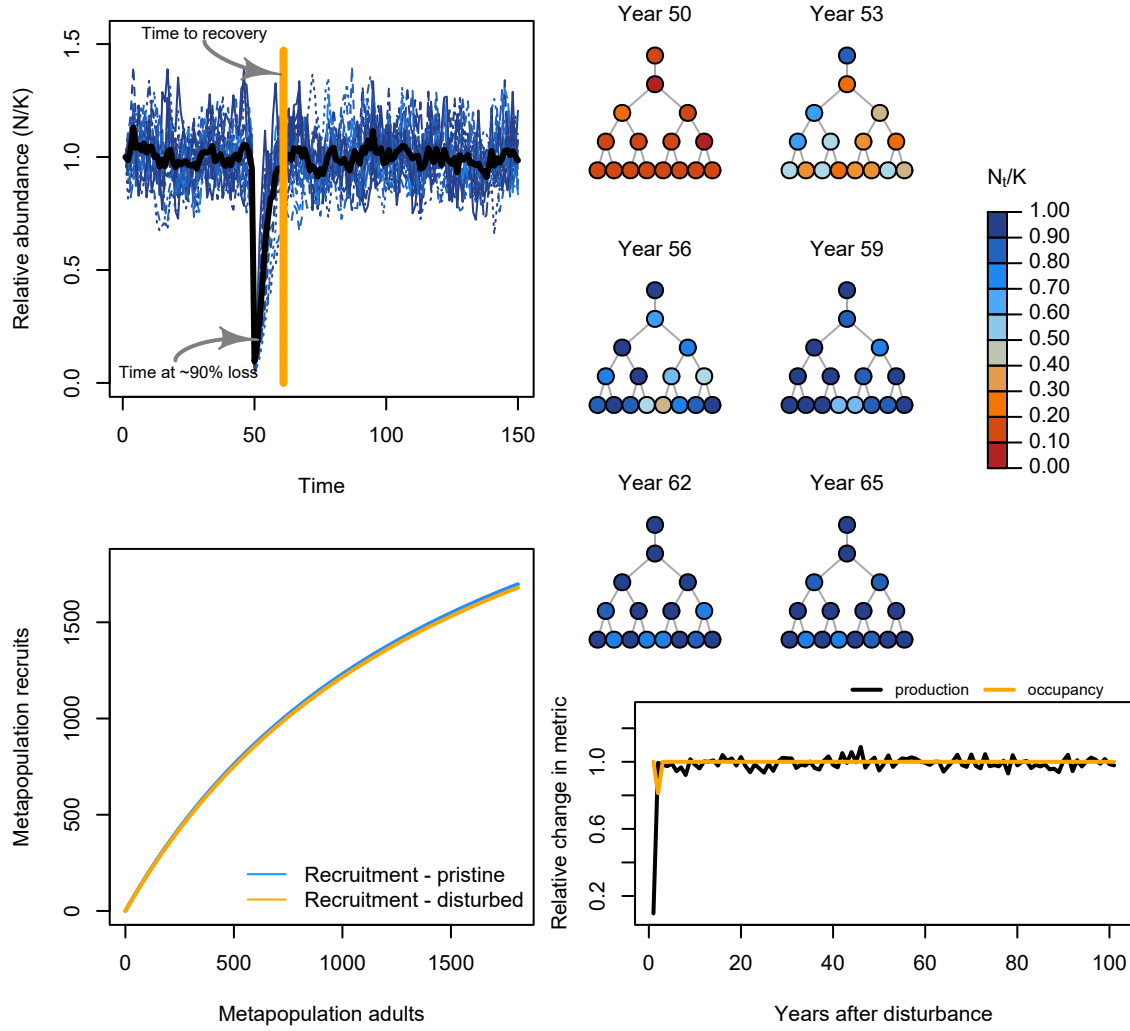


Figure S9: Example iteration of spatial recovery regime of stochastic metapopulation.

<sup>181</sup> Next, we can contrast with a disturbance regime where the disturbance is locally even among a subset of local  
<sup>182</sup> patches (rather than uniform across all patches or local extirpations).

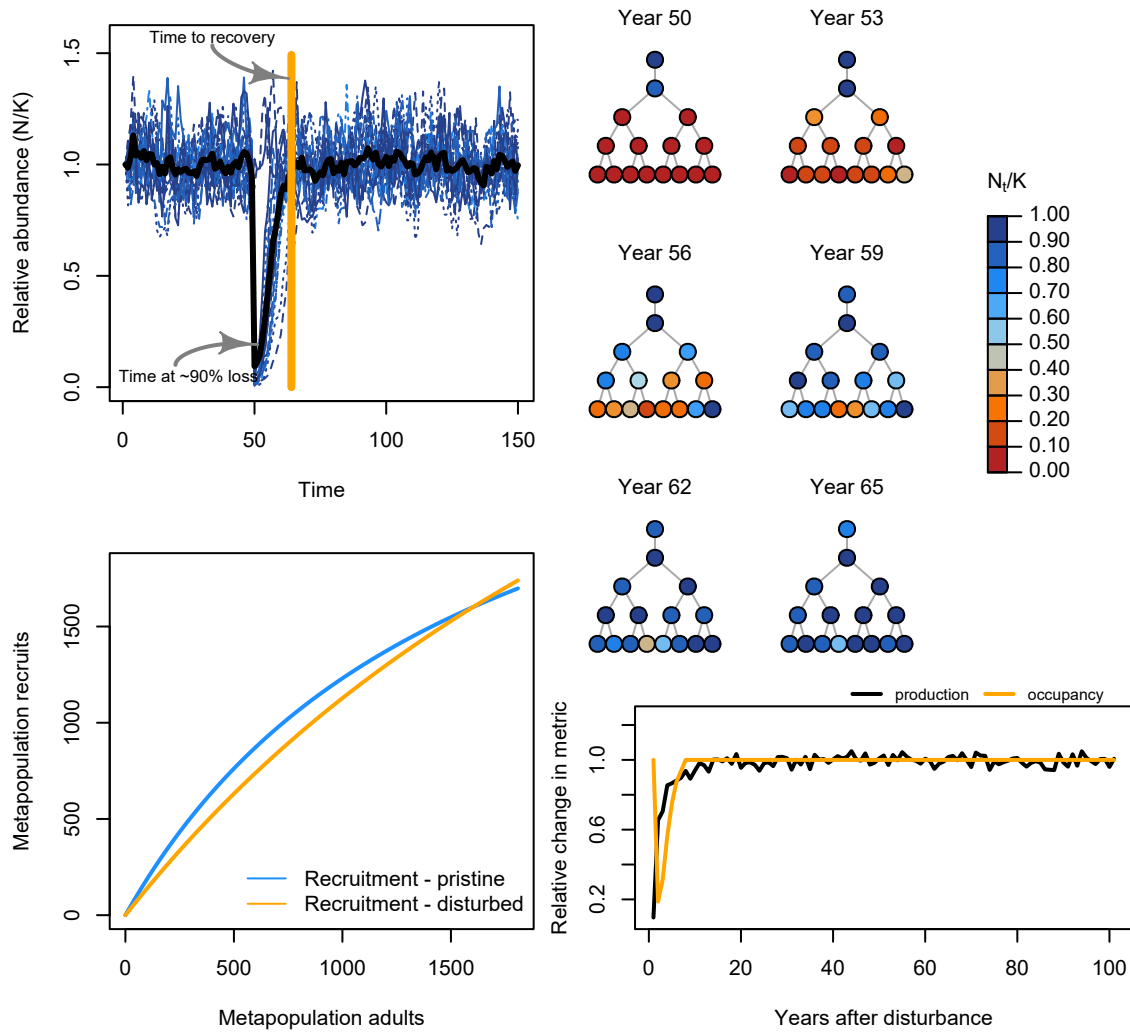


Figure S10: Example iteration of spatial recovery regime of stochastic metapopulation.

183 Next, we can contrast with a disturbance regime where the disturbance is concentrated on local patches that can  
 184 be completely extirpated (rather than the disturbance being applied proportionally across all patches e.g., a  
 185 mixed-stock fishery).

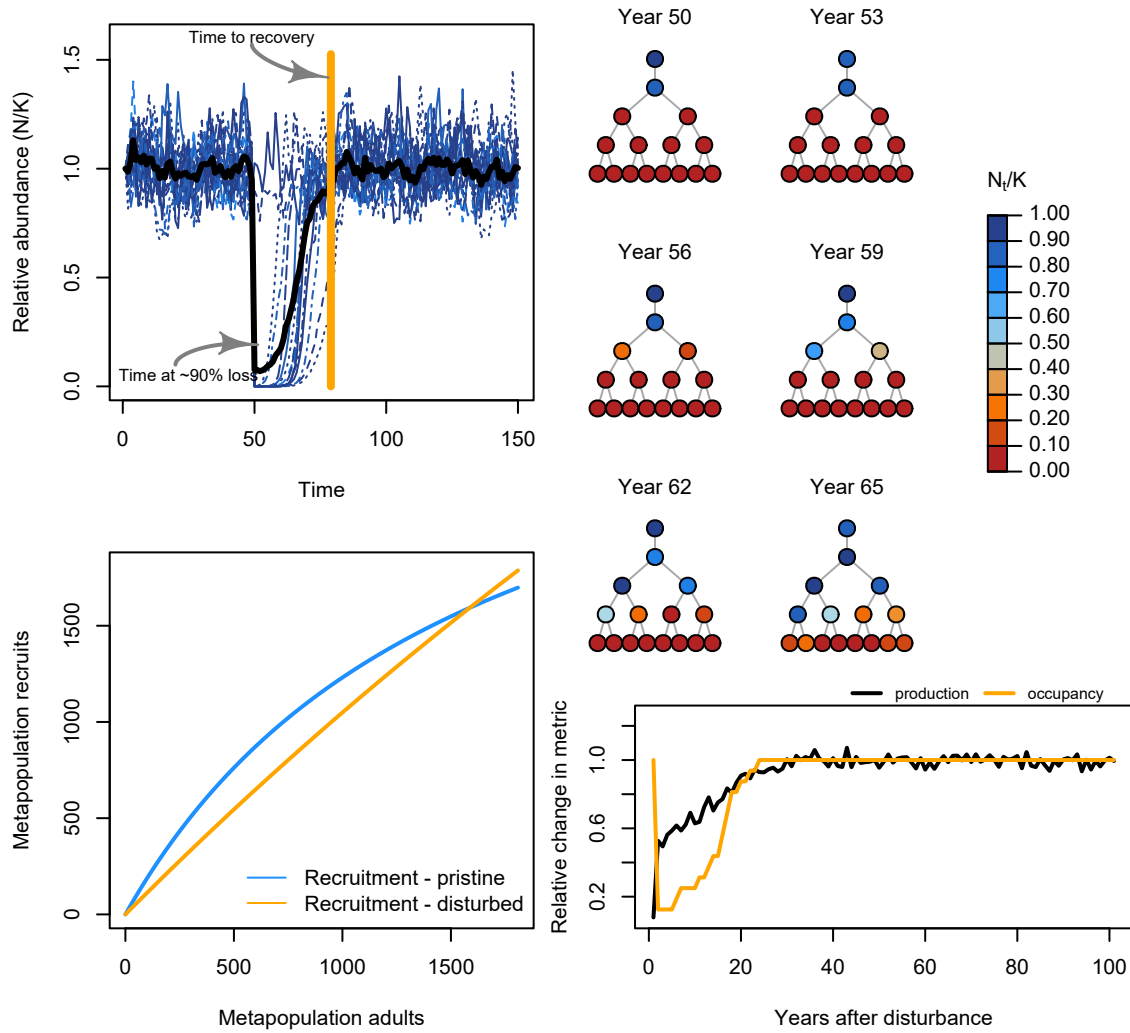


Figure S11: Example iteration of spatial recovery regime of stochastic metapopulation.

#### 186 S1.4 Sensitivity test of mean recovery metrics

187 The total number of scenarios resulted in a long computation time to run all simulations a large number of times  
 188 necessary to evaluate how metapopulation responded, on average, to our ecological and disturbance scenarios. To  
 189 determine a sufficient number of bootstrap iterations to run, we ran a sensitivity test to explore the relative  
 190 sensitivity of the mean for a few recovery metrics of interest (recovery rate) to the number of stochastic simulations  
 191 ran per scenario. Below, we repeated the scenario for a metapopulation with a dendritic network, with high  
 192 stochasticity, locally uneven disturbances, large spatial-temporal correlations, variable patch productivities, and  
 193 variable patch capacities along gradients of 10, 100, 500, and 1,000 stochastic simulations. Based on these  
 194 preliminary results, we see that the mean for most metrics was relatively insensitive with at least 100 simulations.

### Average recovery metrics

#### Sensitivity of mean recovery metrics to the number of stochastic simulations

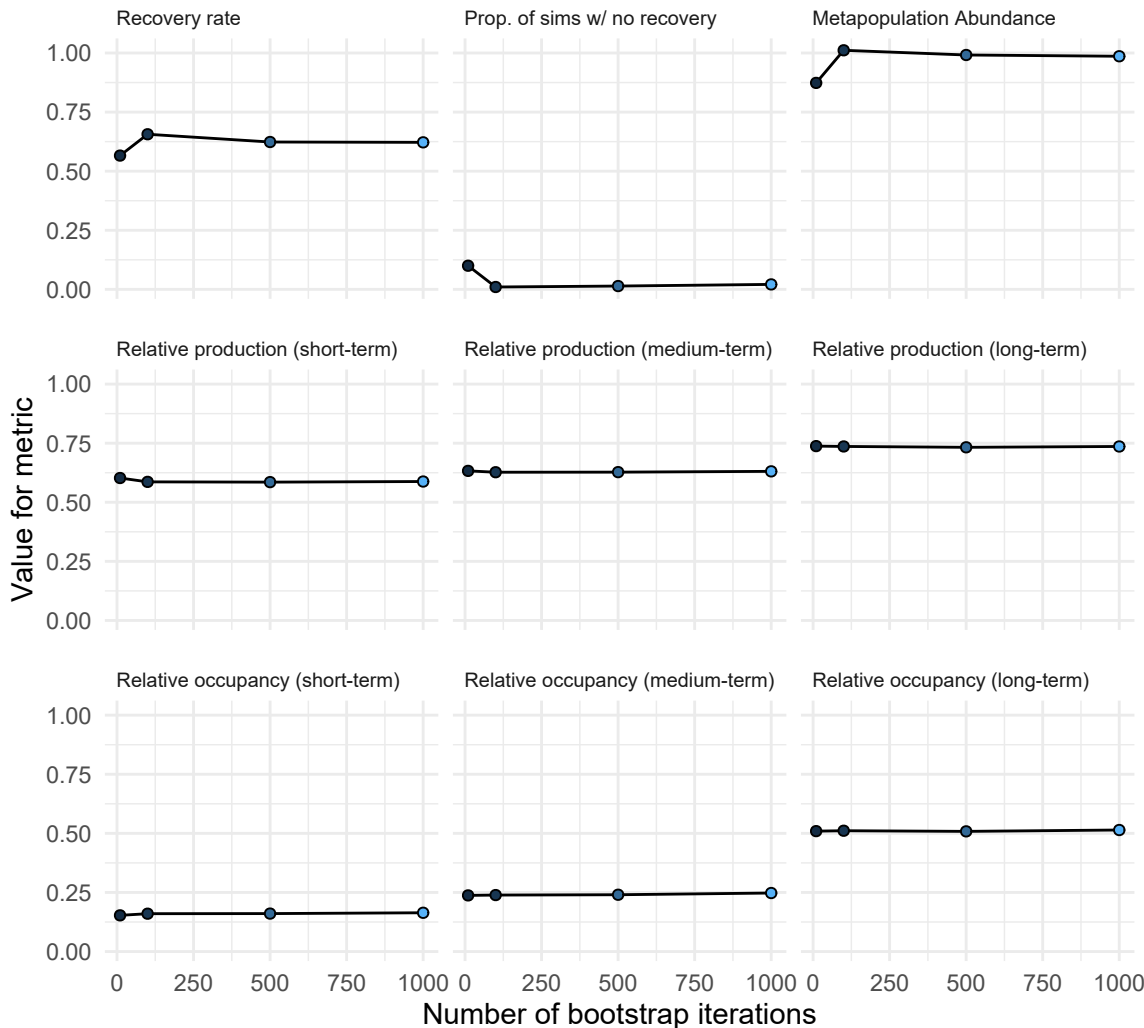


Figure S12: Sensitivity test of mean recovery metrics to number of iterations to bootstrap the stochastic simulations. Example metapopulation consisted of a dendritic network, high recruitment stochasticity, locally uneven disturbance regime, large spatial-temporal correlations, variable patch productivities, and variable patch capacities tested along gradients of 10, 100, 500, and 1,000 bootstrapped iterations.

## 195 S1.5 General patterns

### 196 S1.5.1 Effects of disturbance regime

197 The strongest lever influencing recovery in our simulated metapopulations was, by far, the characteristics of the  
 198 disturbance regime. Specifically, the degree to how locally concentrated the disturbance was on the set of patches  
 199 was more influential than variation in local demographic rates, dispersal rates, or network topology. Localized  
 200 disturbances increased the risk of spatial contraction, reduced recovery rates and aggregate compensation, and  
 201 increased the risk of non-recoveries. By altering aggregate compensation, localized disturbance reduced the relative  
 202 production of the metapopulation. In other words, through changes in source-sink dynamics, metapopulations  
 203 under localized disturbance acted less than the sum of their parts – the more localized the impacts, the worse these  
 204 effects. Uniform disturbances generally left the metapopulation dynamics unaffected with few changes to recovery  
 205 metrics outside of occasionally slower recoveries. These above spatial and temporal recovery processes also  
 206 appeared tied to one another such that changes to any of them had feedbacks with other recovery metrics. Perhaps  
 207 intuitively, for example, patch occupancy was highly correlated to the relative production of the metapopulation,  
 208 such that the more patches occupied, the more that metapopulation dynamics resembled a contiguous population.

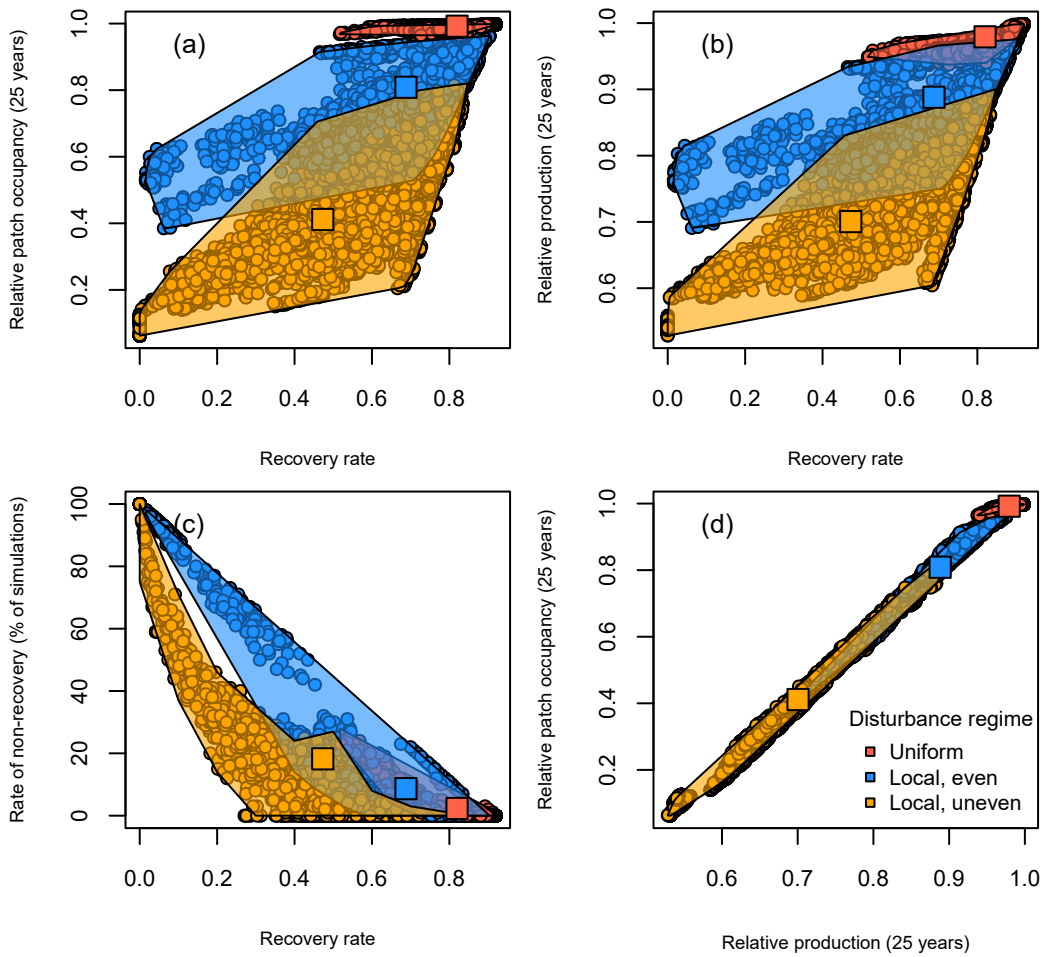


Figure S13: The role of spatial disturbance regimes on metapopulation recoveries and covariation among four recovery metrics: (a,b,c) recovery rate – the annual rate of metapopulation recovery; (a,d) relative patch occupancy – the mean proportion of patches occupied 25 years after disturbance; (b,d), relative production – the ratio between the summed abundances across all patches to the expected production of an equivalent single population 25 years after disturbance; and (c) rate of non-recovery – the percent of 100 stochastic simulations where the metapopulation failed to recover. Each point represents a single simulation for a metapopulation under a unique combination of local productivity, dispersal, spatial network, stochasticity, and disturbance (9,504 total simulations). Shaded regions describe the range in recovery metrics for all simulated metapopulations and are colored by disturbance regime. Square points represent the mean recovery metrics from all simulations within each disturbance regime.

**S1.5.2 Role of network structure & dispersal**

We now show some general patterns in how variable patch demographic rates, network structure, dispersal, disturbance, recruitment stochasticity, and spatio-temporal correlations variation affects metapopulation *recovery rates* (shown in Figure 4 of the main text and Figure S13), *non-recovery rate* (i.e., the number of simulations where the metapopulation fails to recover; Figure S14), *patch occupancy* (i.e., number of patches with local abundance  $<10\%$  of pre-disturbance; Figure S15), and *relative production* (Figure S16).

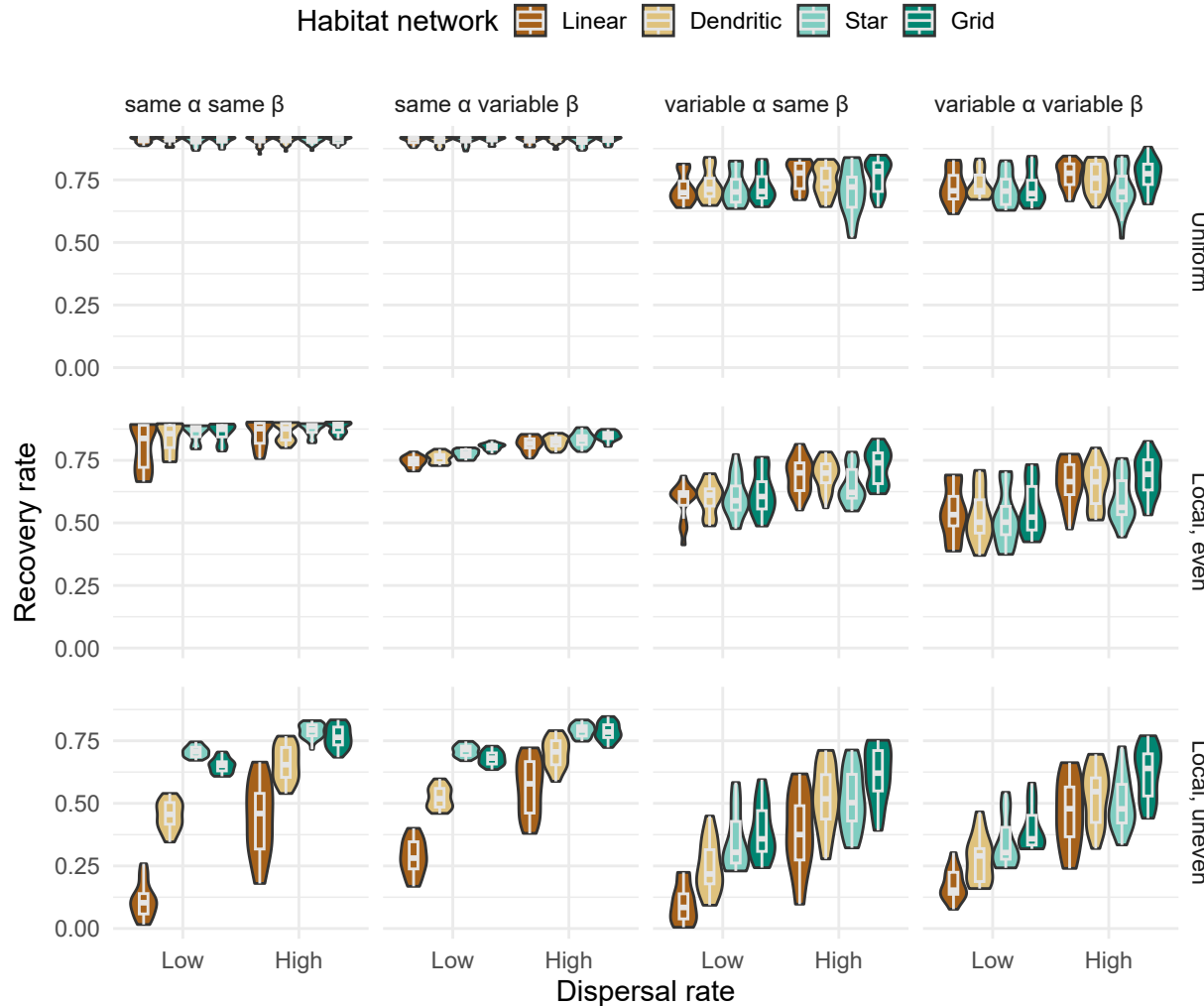


Figure S14: Violin plots showing marginal response of metapopulation recovery rates along gradients of network configuration, dispersal categories (low 0.001; high  $>0.001$ ), heterogeneity in local demographic rates ( $\alpha$  was local patch productivity and  $\beta$  was local patch carrying capacity in the Beverton-Holt model), and spatial distribution of disturbance.

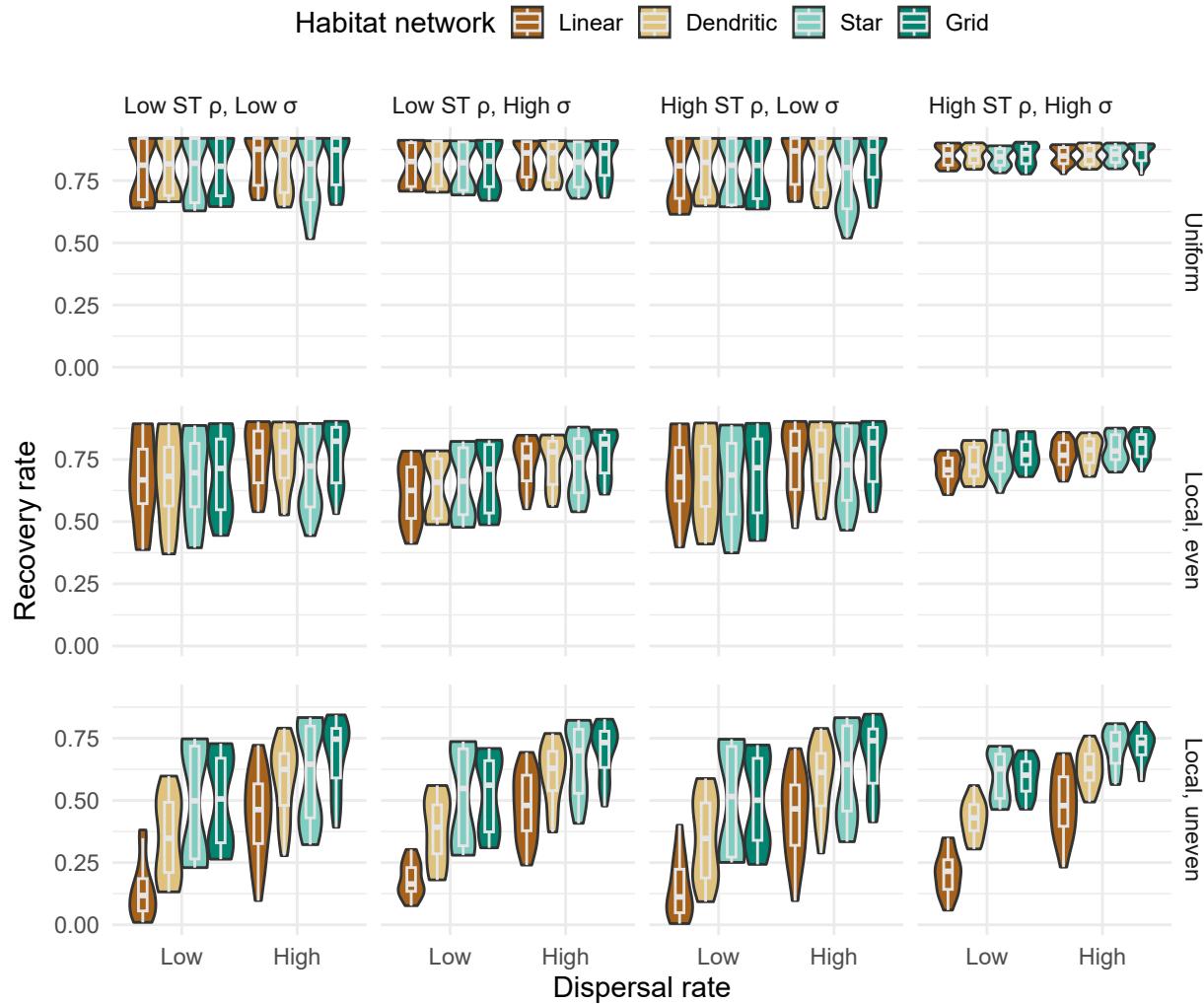


Figure S15: Violin plots showing marginal response of metapopulation recovery rates along gradients of network configuration, dispersal categories (low  $0.001$ ; high  $>0.001$ ), spatial-temporal (ST) correlations (low  $\rho=0$ ; high  $\rho=0.6$ ), scale of lognormal variance in recruitment (low  $\sigma=0.001$ ; high  $\sigma=0.1$ ), and spatial distribution of disturbance .

215 Next, we show violin plots demonstrating some of the modulating factors leading to variation in the risk of  
 216 non-recovery owing to stochastic recruitment dynamics.

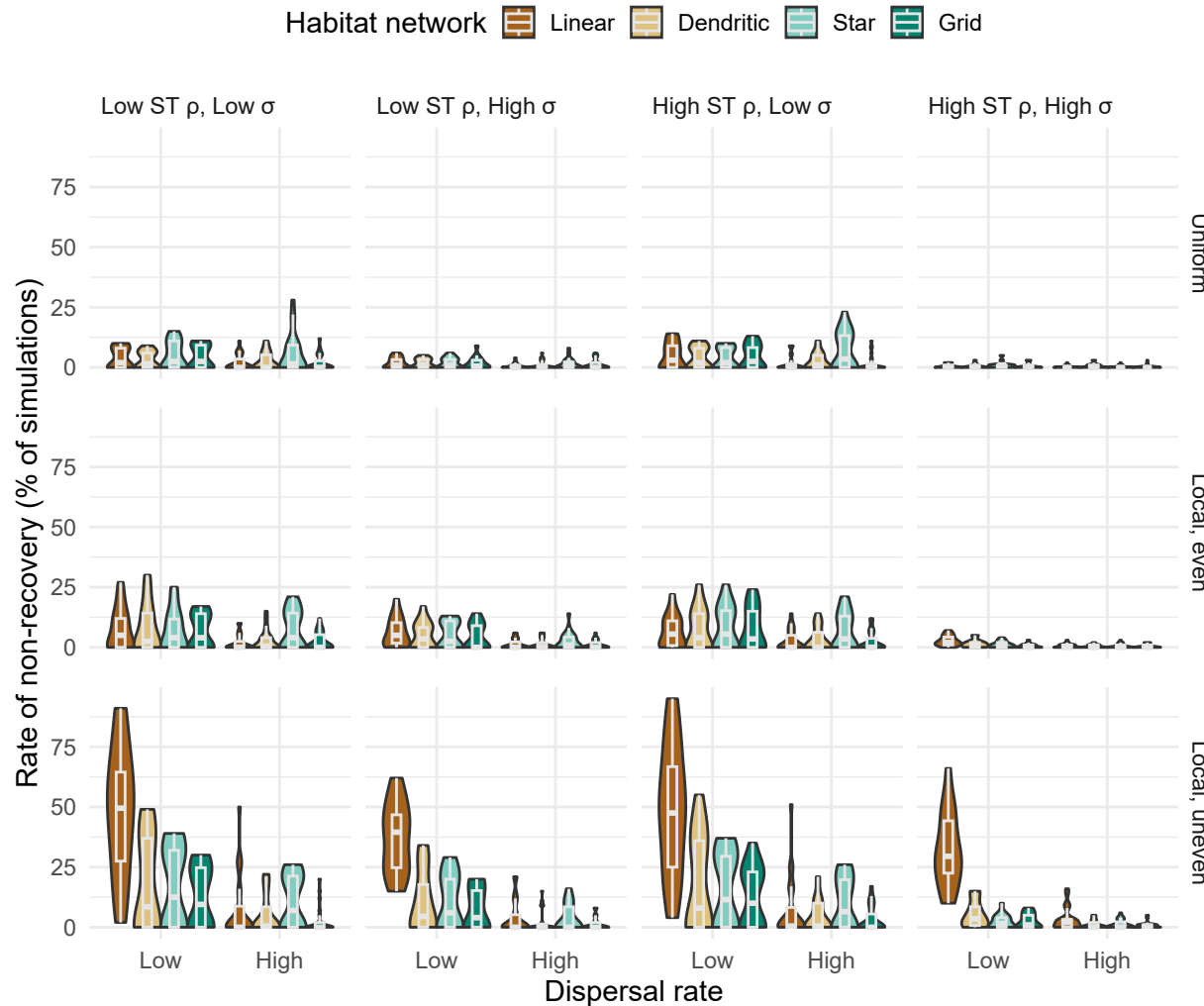


Figure S16: Violin plots showing marginal response of the stochastic risk of non-recovery in metapopulations along gradients of network configuration, dispersal categories (low  $0.001$ ; high  $>0.001$ ), spatial-temporal (ST) correlations (low  $\rho=0$ ; high  $\rho=0.6$ ), scale of lognormal variance in recruitment (low  $\sigma=0.001$ ; high  $\sigma=0.1$ ), and spatial distribution of disturbance.

217 Next, we show violin plots demonstrating some of the modulating factors leading to variation in long-term impacts  
 218 to patch occupancy.

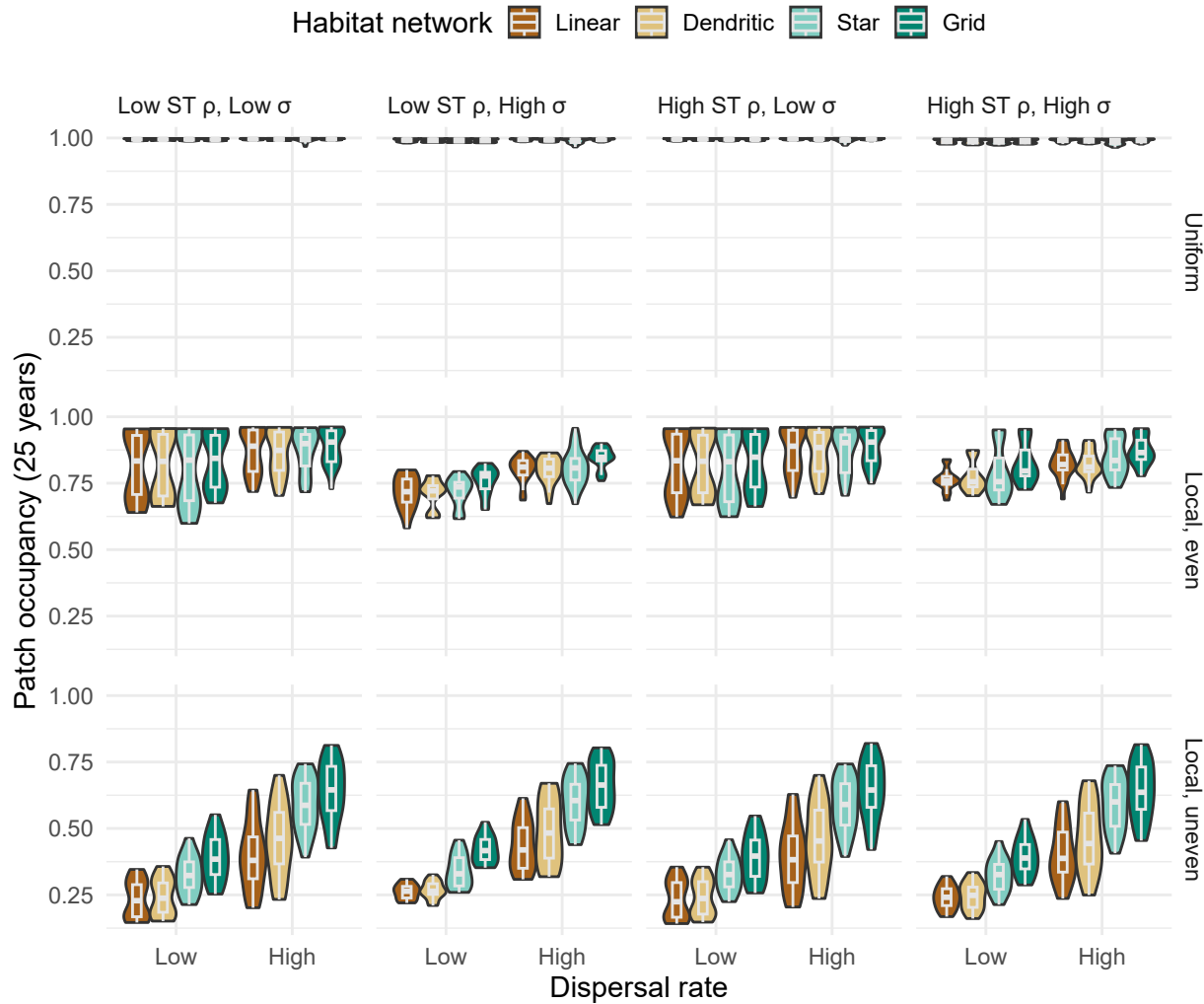


Figure S17: Violin plots showing marginal response of long-term patch occupancy in metapopulations along gradients of network configuration, dispersal categories (low 0.001; high  $> 0.001$ ), spatial-temporal (ST) correlations (low  $\rho = 0$ ; high  $\rho = 0.6$ ), scale of lognormal variance in recruitment (low  $\sigma = 0.001$ ; high  $\sigma = 0.1$ ), and spatial distribution of disturbance.

<sup>219</sup> Next, we show variation in relative production metrics. Figure S12 shows the tight correlation between patch  
<sup>220</sup> occupancy and relative production. Hence, Figure S15 and S16 look quite similar.

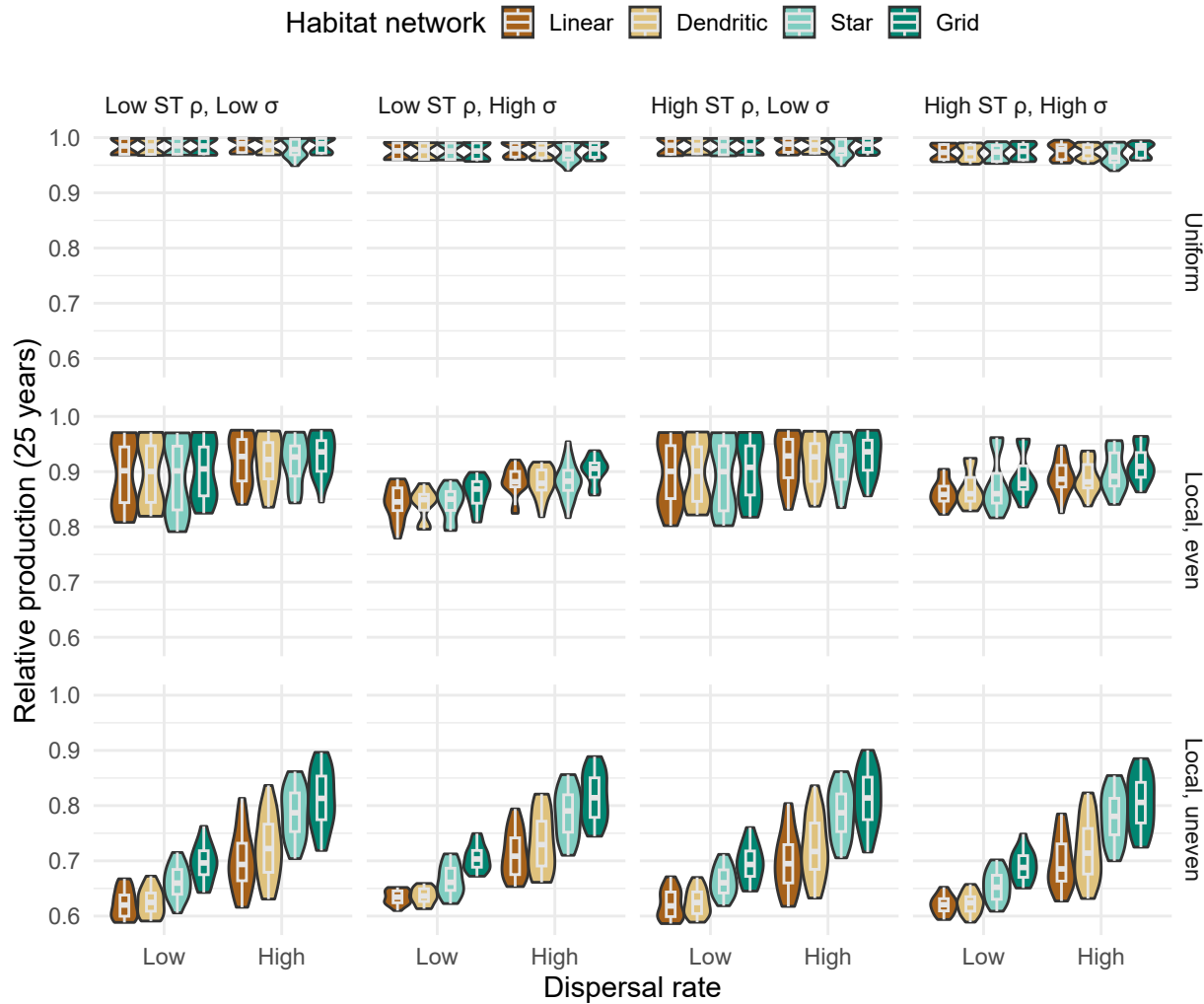


Figure S18: Violin plots showing marginal response of relative production for metapopulations along gradients of network configuration, dispersal categories (low 0.001; high  $> 0.001$ ), spatial-temporal (ST) correlations (low  $\rho = 0$ ; high  $\rho = 0.6$ ), scale of lognormal variance in recruitment (low  $\sigma = 0.001$ ; high  $\sigma = 0.1$ ), and spatial distribution of disturbance.

221 Dispersal, landscape structure, and local density-dependence also affected metapopulation recovery patterns in  
 222 three key ways, though to a lesser extent. First, recovery rates increased with increased dispersal. However, this  
 223 effect was nonlinear with diminishing benefits of dispersal occurring at ~1-3%, depending on spatial structure and  
 224 disturbance. Second, more linearized networks had slower recovery times than more connected networks suggesting  
 225 that rescue effects take some time to cascade through the entire network of patches; but this interacted with the  
 226 disturbance regime as only local, extirpation exhibited this change in any substantial manner. Last, diversity in  
 227 local patch compensation and carrying capacities tended to slow metapopulation recoveries - this effect interacted  
 228 with other factors like stochasticity.

229 **S1.5.3 Clustering analyses**

230 We used hierarchical clustering analyses (implementing Ward's criterion) of a dissimilarity matrix from our four  
 231 recovery metrics to evaluate whether there was evidence for common recovery regimes among our simulation results  
 232 across all ecological and disturbance scenarios (Murtagh & Legendre 2014). Based on advice laid out in Hennig  
 233 (2014), we determined that the best number of unique clusters in metapopulation recoveries should satisfy the  
 234 following statistical criteria:

- 235 1. recovery outcomes from within a cluster are closer to one another than to other clusters (i.e., the two Dunn  
 236 indices are relatively high)  
 237 2. the number of clusters explains much of the point variation within the dataset (i.e., diminishing returns in  
 238 minimizing the sums-of-squared residuals)  
 239 3. the point observations within clusters are relatively tight (i.e., both the average silhouette width and the  
 240 widest within-cluster gap are relatively low)  
 241 4. clusters are relatively unique and there is good separation between the clusters (i.e., the separation index is  
 242 still high, while considering that low numbers of clusters should always have the highest separation)

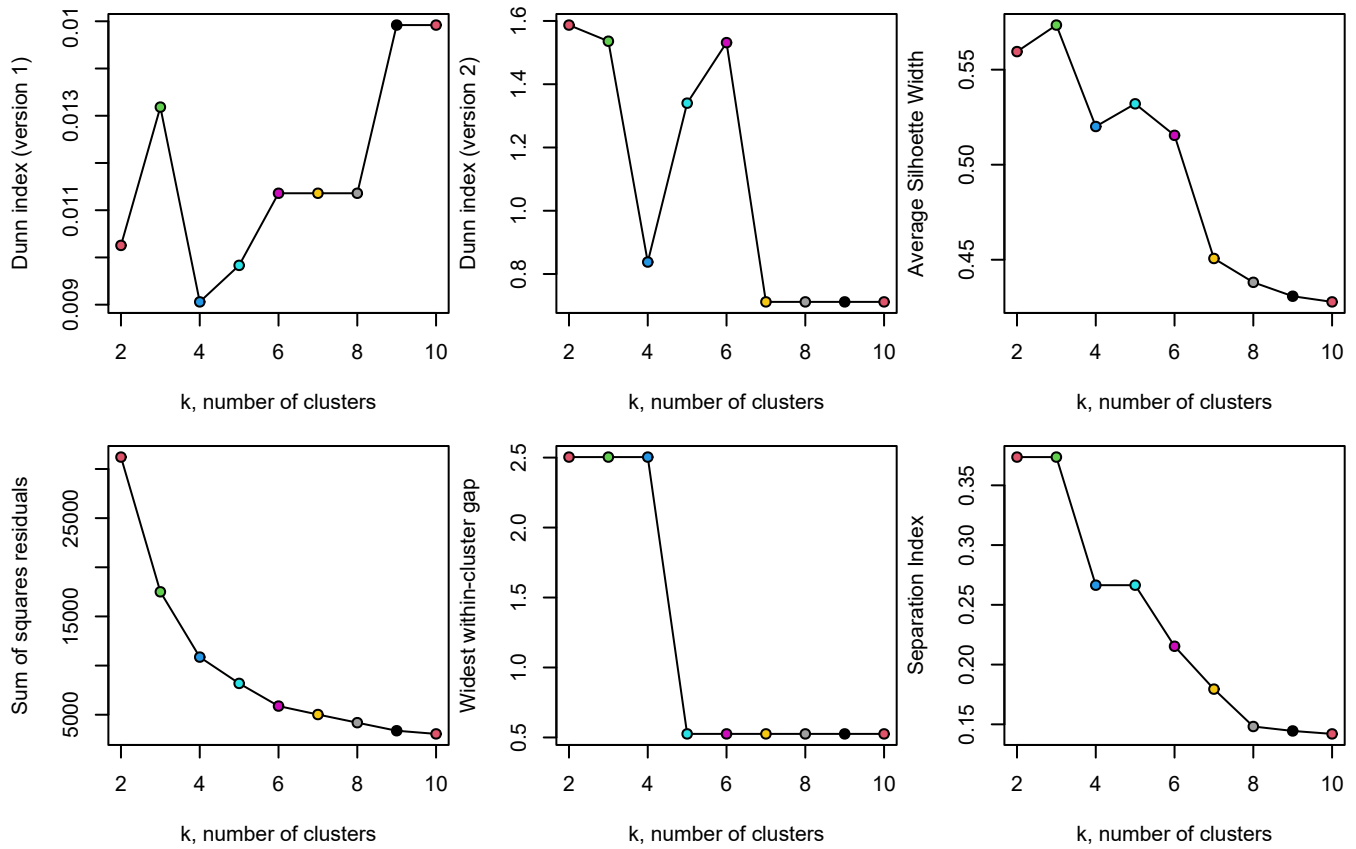


Figure S19: The relationships between number of potential clusters and multiple statistical criteria used to test support for the best number of clusters within the simulated recovery outcomes

243 Based on the above criteria, we chose 5 unique clusters as satisfying most of the above criteria in the figure above,  
 244 although there was good support for between 3 and 6 unique clusters. The principal components analysis indicates  
 245 that five clusters has substantial explanatory power of metapopulation recovery metrics (explained ~89% of the  
 246 point variation).

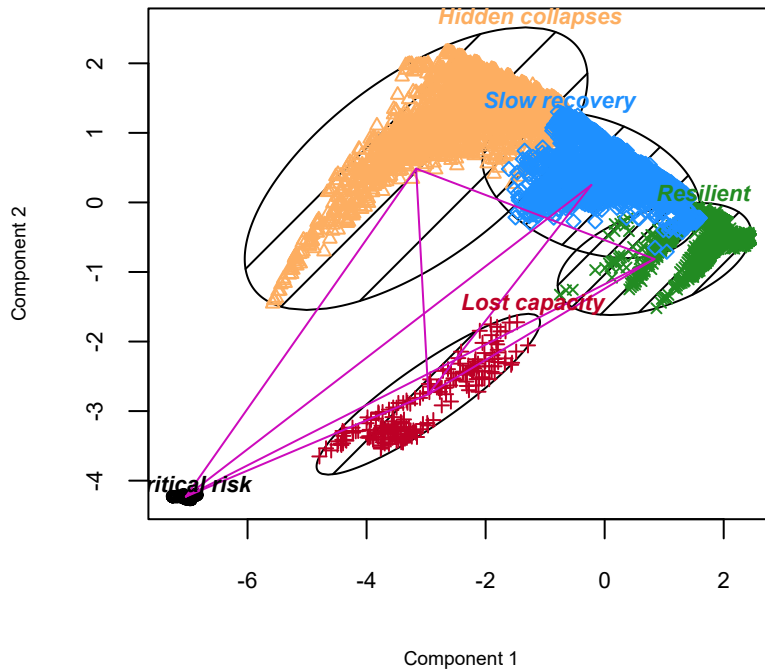


Figure S20: Bivariate cluster plot of the principal components explaining point variation in metapopulation recovery metrics across all simulated scenarios grouped into five distinct clusters.

#### 247 S1.5.4 Emergent recovery outcomes

248 Overall, we used hierarchical clustering analyses to describe five common metapopulation recovery outcomes. These  
 249 outcomes were: (1) resilient recovery – metapopulations recovered to pre-disturbance abundances quickly with all  
 250 patches occupied, (2) slow recovery – were either slowed (compared to resilient recoveries), had reduced patch  
 251 occupancy, or reduced relative production, (3) hidden collapses – metapopulations tended to recover and aggregate  
 252 abundances were high, but many local patches remained unoccupied and recovery was slowed, (4) lost capacity –  
 253 recovery rates were very slow, the risk of non-recovery was high, long-term production was low, and many local  
 254 patches remained unoccupied and (5) critical risk – where metapopulations failed to recover, abundances remained  
 255 low, and the risk of non-recovery was high.

Table S2: The mean recovery metrics, total sample size per regime (No.), and metapopulation abundance (N/K) for each of five common metapopulation recovery regimes supported by hierarchical clustering analyses across gradients in disturbance and network structure.

Regime	Network	Disturbance	No.	Recovery rate	% non-recovery	Occupancy	Relative production	Relative abundance
Resilient	Linear	Uniform	792	0.83	2	0.99	0.98	1.00
Resilient	Dendritic	Uniform	792	0.82	2	0.99	0.98	0.99
Resilient	Star	Uniform	792	0.81	3	0.99	0.98	0.99
Resilient	Grid	Uniform	792	0.82	2	0.99	0.98	1.00
Resilient	Linear	Local, even	205	0.78	5	0.94	0.95	0.99
Resilient	Dendritic	Local, even	201	0.78	5	0.94	0.96	0.99
Resilient	Star	Local, even	274	0.75	7	0.93	0.95	0.99
Resilient	Grid	Local, even	215	0.78	5	0.94	0.96	0.99
Slow recovery	Linear	Local, even	528	0.69	3	0.77	0.87	0.99
Slow recovery	Dendritic	Local, even	533	0.70	3	0.77	0.87	0.99

Slow recovery	Star	Local, even	466	0.68	5	0.75	0.86	0.99
Slow recovery	Grid	Local, even	529	0.73	3	0.81	0.89	0.99
Slow recovery	Linear	Local, uneven	11	0.72	0	0.64	0.81	1.00
Slow recovery	Dendritic	Local, uneven	69	0.73	0	0.66	0.81	0.99
Slow recovery	Star	Local, uneven	114	0.74	4	0.71	0.84	0.97
Slow recovery	Grid	Local, uneven	244	0.76	0	0.73	0.85	1.00
Hidden collapses	Linear	Local, even	9	0.61	3	0.59	0.79	0.99
Hidden collapses	Dendritic	Local, even	9	0.65	0	0.59	0.78	0.99
Hidden collapses	Star	Local, even	4	0.72	0	0.55	0.76	1.00
Hidden collapses	Linear	Local, uneven	709	0.34	21	0.34	0.67	0.97
Hidden collapses	Dendritic	Local, uneven	651	0.49	8	0.36	0.68	0.99
Hidden collapses	Star	Local, uneven	606	0.57	9	0.45	0.72	0.99
Hidden collapses	Grid	Local, uneven	476	0.56	7	0.46	0.73	0.99
Lost capacity	Linear	Local, even	50	0.17	77	0.58	0.79	0.66
Lost capacity	Dendritic	Local, even	49	0.16	78	0.58	0.78	0.65
Lost capacity	Star	Local, even	48	0.16	78	0.58	0.78	0.65
Lost capacity	Grid	Local, even	48	0.16	79	0.57	0.78	0.64
Critical risk	Linear	Local, uneven	72	0.00	100	0.10	0.54	0.09
Critical risk	Dendritic	Local, uneven	72	0.00	100	0.10	0.54	0.08
Critical risk	Star	Local, uneven	72	0.00	100	0.10	0.54	0.08
Critical risk	Grid	Local, uneven	72	0.00	100	0.10	0.54	0.08

256 In general, the five recovery regimes spanned a continuum of better (e.g., resilient) to worse recoveries (e.g.,  
 257 long-term critical risks). Overall, the interplay between ecological and disturbance conditions appeared to structure  
 258 the specific pathway for metapopulation recoveries (Figure S19; Table S2). For example, uniform disturbances  
 259 always led to resilient recoveries. However, local, even disturbance regimes tended to lead to, at-best, a resilient  
 260 recovery or, at worst, hidden collapses with the probability modulated by other ecological factors. Local, uneven  
 261 disturbance regimes led to, at best, a slow recovery or, at worst, a long-term critical risk and non-recovery. The  
 262 main text Figure 5 and 6 demonstrates the conditions that led to resilient recoveries compared to critical risks,  
 263 while more intermediate outcomes, like slow recovery, hidden collapses, or lost capacity are shown here in Figures  
 264 S20-S22.

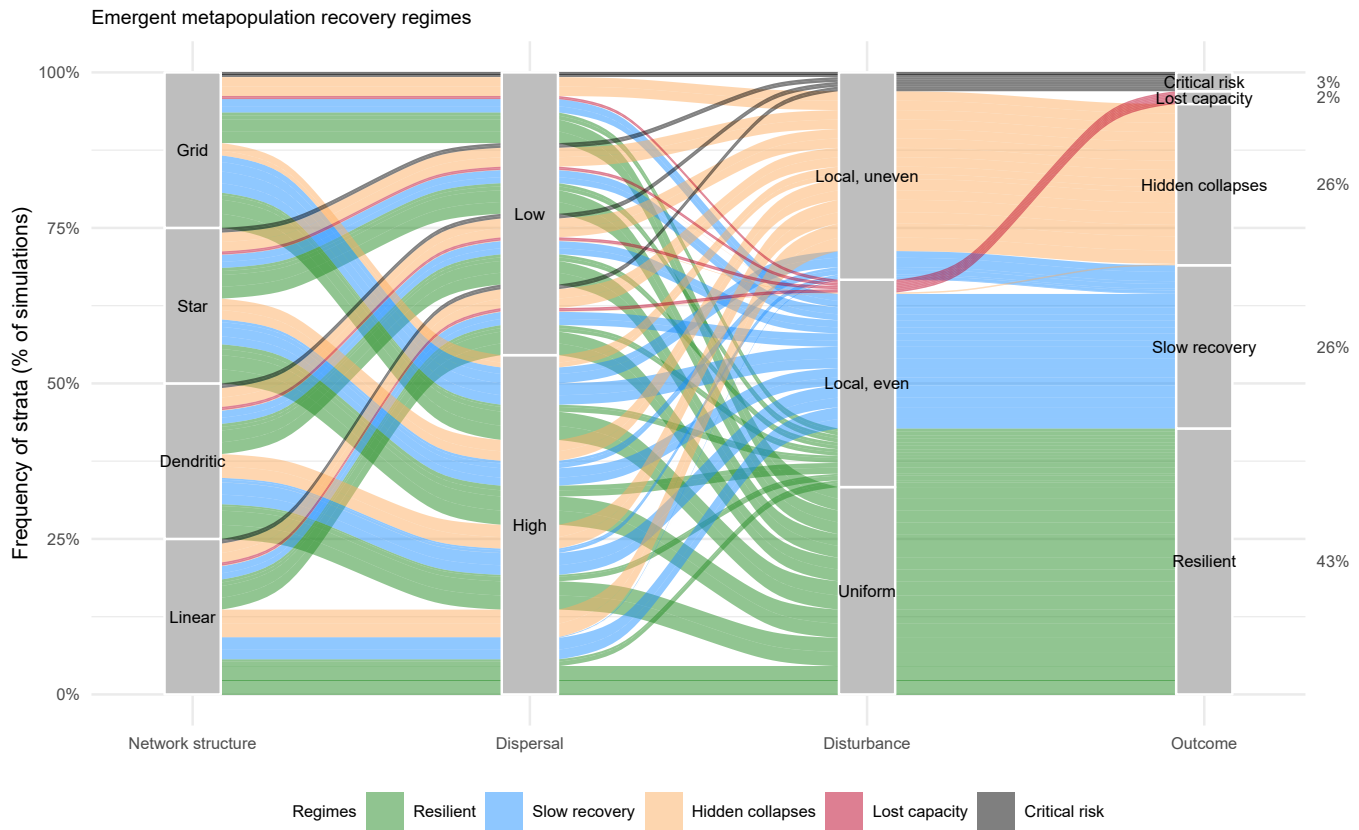


Figure S21: Frequency of emergent metapopulation recovery regimes can depend on a complex interplay between network structure, dispersal, and spatial disturbances. Ribbon colors denote a group of simulations that led to one of five common recovery outcomes. Frequency of regimes denoted by width of ribbons

265 Local patch demography, habitat network structure, dispersal, spatially and temporally correlated recruitment  
 266 variation, and spatial disturbance regimes each had modulating effects on the probability for any particular  
 267 recovery regime (Figures 5 & 6 in the main text; and Figures S20-S22 here). There was a clear signal from any  
 268 localized disturbances, which increased the probability for non-resilient recovery regimes. For habitat networks,  
 269 metapopulations with linear networks tended to have increased probability for worse recoveries compared to  
 270 gridded networks. For dispersal rates, metapopulations with low dispersal had increased probability for poor  
 271 recoveries compared to high dispersal. For local demography, metapopulations with variable local patch  
 272 demographic rates tended to increased probability for poor recoveries compared to metapopulations composed of  
 273 homogeneous local patches. For recruitment stochasticity, metapopulations with both high recruitment variation  
 274 and high spatial-temporal correlations led to increased probability for poor recoveries compared to low variation  
 275 and low correlations.

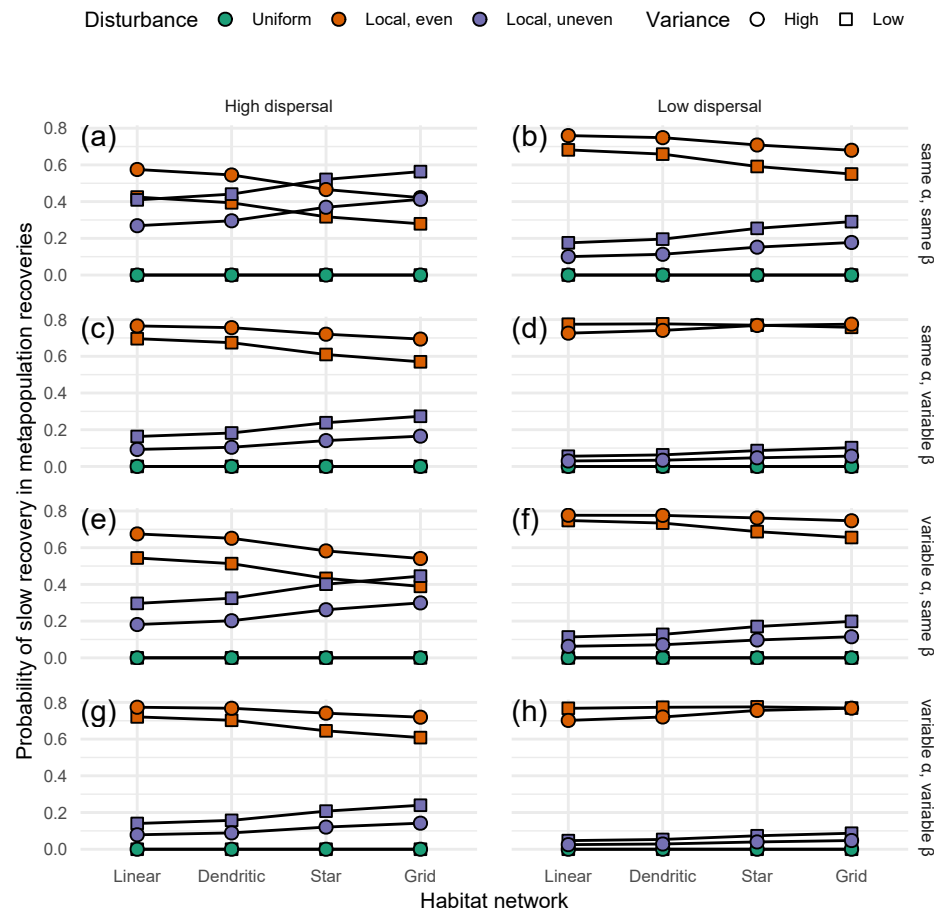


Figure S22: The probability of a slow recovery in metapopulation recoveries depended on the interplay between network structure, dispersal (low  $0.001$ ; high  $>0.001$ ), spatial disturbances, heterogeneity in local demographic rates ( $\alpha$  is local patch productivity and  $\beta$  is local patch carrying capacity), and spatial-temporal recruitment variation (high= $\rho=0.6$  and  $\sigma=0.1$ ; low= $\rho=0$  and  $\sigma=0.001$ ).

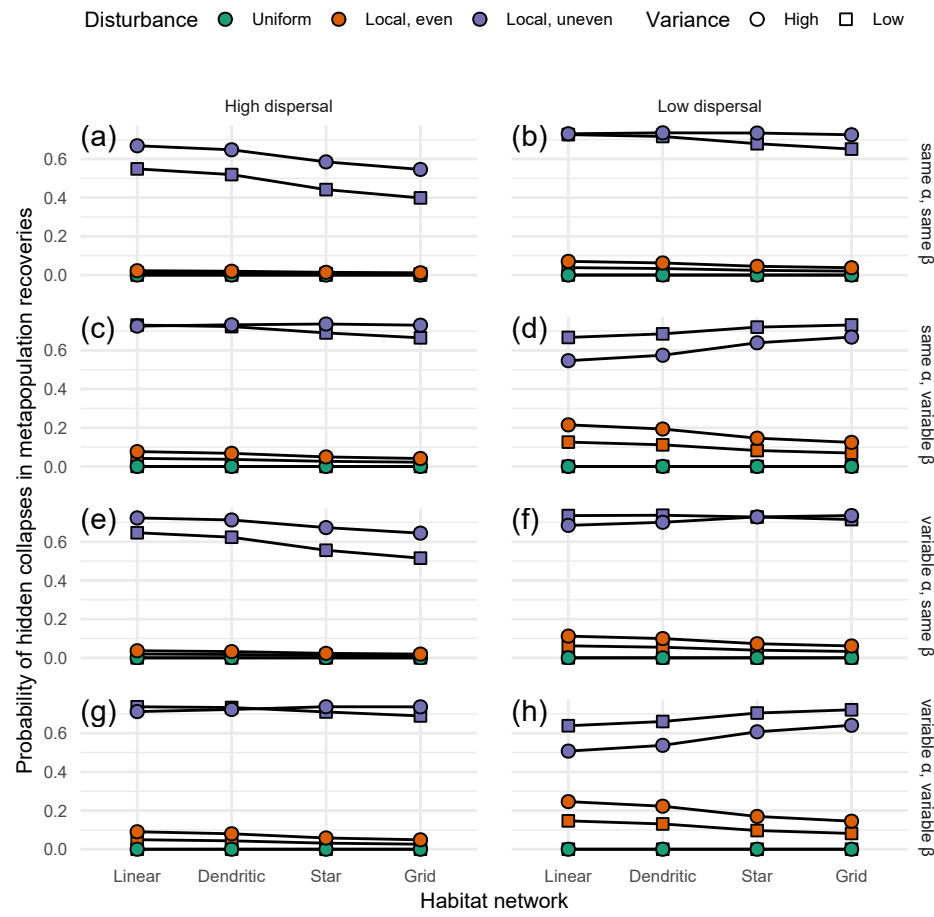


Figure S23: The probability of hidden local collapses in metapopulation recoveries depended on the interplay between network structure, dispersal (low 0.001; high > 0.001), spatial disturbances, heterogeneity in local demographic rates ( $\alpha$  is local patch productivity and  $\beta$  is local patch carrying capacity), and spatial-temporal recruitment variation (high =  $\rho=0.6$  and  $\sigma=0.1$ ; low =  $\rho=0$  and  $\sigma=0.001$ ).

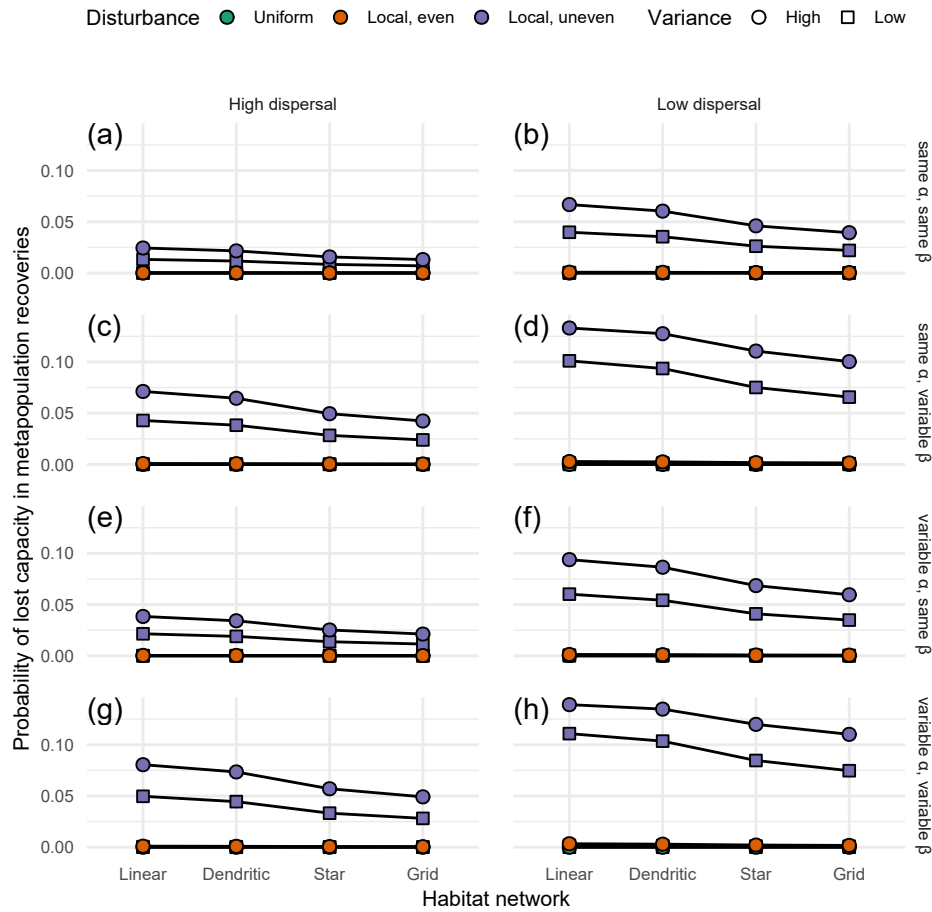


Figure S24: The probability of lost productive capacity in metapopulation recoveries depended on the interplay between network structure, dispersal (low 0.001; high > 0.001), spatial disturbances, heterogeneity in local demographic rates ( $\alpha$  is local patch productivity and  $\beta$  is local patch carrying capacity), and spatial-temporal recruitment variation (high =  $\rho=0.6$  and  $\sigma=0.1$ ; low =  $\rho=0$  and  $\sigma=0.001$ ).

## S1.6 References

- Anderson, S.C., Moore, J.W., McClure, M.M., Dulvy, N.K. & Cooper, A.B. (2015). Portfolio conservation of metapopulations under climate change. *Ecological Applications*, 25, 559–572.
- Bowlby, H.D. & Gibson, A.J.F. (2020). Evaluating whether metapopulation structure benefits endangered diadromous fishes. *Canadian Journal of Fisheries and Aquatic Sciences*, 77, 388–400.
- Csardi, G. & Nepusz, T. (2006). The igraph software package for complex network research. *InterJournal, Complex Sy*, 1695.
- Forrest, R.E., McAllister, M.K., Dorn, M.W., Martell, S.J.D. & Stanley, R.D. (2010). Hierarchical Bayesian estimation of recruitment parameters and reference points for Pacific rockfishes (*Sebastodes* spp.) under alternative assumptions about the stock-recruit function. *Canadian Journal of Fisheries and Aquatic Sciences*, 67, 1611–1634.
- Fullerton, A.H., Anzalone, S., Moran, P., Van Doornik, D.M., Copeland, T. & Zabel, R.W. (2016). Setting spatial conservation priorities despite incomplete data for characterizing metapopulations. *Ecological Applications*, 26, 2558–2578.
- Hennig, C. (2014). How many bee species? A case study in determining the number of clusters. In: *Data analysis, machine learning and knowledge discovery* (eds. Spiliopoulou, M., Schmidt-Thieme, L. & Janning, R.). pp. 41–49.
- Moore, J.W., Connors, B.M. & Hodgson, E.E. (2021). Conservation risks and portfolio effects in mixed-stock fisheries. *Fish and Fisheries*, faf.12567.
- Murtagh, F. & Legendre, P. (2014). Ward's hierarchical agglomerative clustering method: which algorithms implement Ward's criterion? *Journal of Classification*, 31, 274–295.
- Myers, R.A., Bowen, K.G. & Barrowman, N.J. (1999). Maximum reproductive rate of fish at low population sizes. *Canadian Journal of Fisheries and Aquatic Sciences*, 56, 2404–2419.

- 299 Okamoto, D.K., Hessing-Lewis, M., Samhouri, J.F., Shelton, A.O., Stier, A.C., Levin, P.S. & Salomon, A.K. (2020).  
300 Spatial variation in exploited metapopulations obscures risk of collapse. *Ecological Applications*, 30, e02051.  
301 Walters, C.J. & Martell, S.J.D. (2004). *Fisheries ecology and management*. Princeton University Press.  
302 Yeakel, J.D., Moore, J.W., Guimarães, P.R. & Aguiar, M.A.M. de. (2014). Synchronisation and stability in river  
303 metapopulation networks. *Ecology Letters*, 17, 273–283.  
304 Zelnik, Y.R., Arnoldi, J. & Loreau, M. (2019). The three regimes of spatial recovery. *Ecology*, 100, e02586.